Alma Mater Studiorum · University of Bologna

School of Science
Department of Physics and Astronomy
Master Degree in Physics

Sub-GeV Hadrophilic Dark Matter at Neutrino Detectors

Supervisor:
Dr. Filippo Sala

Co-supervisor:
Prof. Silvia Pascoli

Submitted by:
Francesco Xotta

Academic Year 2022/2023

ABSTRACT

Despite its success in explaining a wide range of phenomena, the Standard Model is unable to elucidate the nature of dark matter, that remains yet unknown, and is then considered to be incomplete.
In this thesis we extensively investigate the parameter space for a light Sub-GeV hadrophilic candidate of dark matter that couples to the up-quark through a scalar mediator, exploring its phenomenology and the limits from literature for this candidate of dark matter.
We study the production from air showers initiated by primary cosmic rays colliding with the atmosphere, obtaining the interactions with mesons through chiral perturbation theory. We consider the decay of the η meson both on-shell and off-shell, allowing us to increase the mass of the mediator freely, covering previously unexplored regions of the parameter space.
By using Super-Kamiokande, Xenon-1T and KamLAND data we place the world-leading limits on different regions of the parameter space, where we also derive sensitivities for JUNO, DUNE, Darwin and Hyper-Kamiokande.
We show that neutrino detectors are particularly important in the detection of light dark matter with mediators with masses higher than ~ 100 MeV while direct detection experiments (such as Xenon1T) are more effective when the mediator is lighter.

Contents

Chapter 1

Introduction

Past astrophysical observations (see [1] in particular) have proved the existence of a matter non visible through light; this matter has been called "dark matter", and was studied extensively in the past years to discover its nature.
Measurements by Planck satellite [2] showed that approximately 95% of the Universe is made either of dark matter or dark energy, which can't be accounted for by the Standard Model (SM) of particle physics and General Relativity (GR) alone, suggesting the need to extend the SM with new particles.
The notion that the standard model is incomplete does not arise only from Dark Matter however, as the Standard Model currently can't explain neutrino masses[3] or the baryon asymmetry of the universe[4]; this implies the possible existence of new particles, that could be at the origin of dark matter.
One of the most important techniques used for the detection of particle dark matter with non gravitational interactions (something that is generally required to explain their production and is a prerequisite for detection [5]) has been Direct detection [6] (with the most researched candidate being Weakly Interactive Massive Particles, with masses from 10 GeV up to 100 TeV [7]). These searches have however detected no dark matter signal ([8, 9, 10]). In addition, the LHC has found no clear sign of the physics beyond the Standard Model that would motivate that mass range[11].

Light Dark Matter with a mass in the MeV-GeV range (similarly to ordinary matter) is in general much less constrained than WIMPs, with interactions to the Standard Model that must proceed through a light mediator to reproduce the observed dark matter abundance[5], while also evading the Tremaine-Gunn bound [12]. If we assume the mass of dark matter as small enough, this class of candidates could also explain the positron excess from the galactic center[13].
Recently, following the lead of [14], [15] and lately [16] have been studying the

possibility that dark matter may be produced from the decay of mesons in baryonic air showers initiated by the impact of cosmic rays on the atmosphere and then detected via the recoils it induces at detectors on Earth. Historically, this is how several particles (examples being the muon[17, 18] and the pion[19]) have been discovered, mainly due to the steady flux produced by atmospheric beam dumps. In this thesis we critically review this detection technique and extend it to new motivated regions of the parameter space by studying for the first time the detection of atmospheric Dark Matter at large neutrino detectors.
The model we consider is an hadrophilic sub-GeV dark matter fermion, that couples with a single flavour of quarks through a scalar singlet mediator (see reference [20]).

In the first chapter, we introduce the concept of dark matter, explaining how it came to be historically; we also expand on the motivations behind Sub-GeV dark matter.
We then introduce the model of hadrophilic sub-GeV dark matter that we are considering (following [20]), showing how we obtain meson couplings to the mediator from the chiral lagrangian (see [21]), the cross section between dark matter and nuclei (showing also the form factors we are going to consider, taken from [22] and [23]) and the phenomenology of this dark matter candidate, including previous limits from the literature (see [23] for a review of them).
In the third chapter a review of the physics behind cosmic rays and air showers is presented; we in particular explain how cosmic rays are accelerated [24], how do they start air showers and how they develop [25].
Finally, in chapter four we show our new limits, explaining how we can obtain the flux for dark matter coming from the atmosphere and how this dark matter interacts with nuclei at detectors, focusing in particular on limits from Xenon1T [9], Super-Kamiokande [26] and KamLAND [27].
We also show sensitivities for DARWIN [28], Hyper-Kamiokande [29], JUNO [30] and DUNE [31].

Chapter 2

Dark Matter

Currently, it is believed that only 5% of the universe is of baryonic nature, with approximately 27% being dark matter and the remaining being dark energy [32], with the latest measures from Planck seeing that the total amount of matter (baryonic and dark) should be approximately 31.7% of the total energy in the universe [2].

In 1933 Fritz Zwicky discovered that the mass of Coma Clusters obtainable from observing the luminous matter was substantially smaller than the mass required to explain the velocity dispersion relation of said cluster [33]; this discovery and the name he gave to this new matter ("dunkle (kalte) materie", that roughly translates to "dark matter") has, erroneously, given Zwicky the paternity of the term "dark matter" (DM).
The term "Dark Matter" however was first used by Henri Poincaré in 1906 and the concept is even older, as it was first discussed by Lord Kelvin![13]
It was however only in the 1980s (see [1]) that astronomers became convinced of the existence of a non luminous matter that made up most of the mass of galaxies and it was then in the beginning of the 21st century that the the "double dark" cosmological model (dark matter and dark energy making up approximately 95% of the energy of the universe) was accepted. Since then the challenge has shifted to understanding the underlying physics of the constituents of dark matter.

2.1 Evidences of Dark Matter

As seen before, evidences for the existence of Dark Matter (DM) have been growing up since 1933. We now show those evidences and explain what led to the acceptance of DM.
For more informations see references [34, 35].

2.1.1 Rotation Curves

One of the most relevant evidences for Dark Matter comes from the rotational velocity v_c of stars in galaxies; evidences for a flat velocity distribution started appearing in the 1970s, but it was in 1980 that the flattening of 21 Sc was first measured [1].

For a rotational motion around the center of the galaxy we should see that from newtonian gravity and assuming spherical symmetry

$$v_c = \sqrt{\frac{GM(r)}{r}} \tag{2.1}$$

Most of the mass in galaxies is located in the galactic disk. For $r > R_{DISK}$ (with R_{DISK} being the radius of the galactic disk) Gauss' Law would tell us that the mass M is constant and, assuming all of the mass is concentrated on the disk, we would see that $v \propto r^{-1/2}$. The rotation speed is instead seen to flatten at large radial distances[1], meaning that the mass is supposed to go as $M(r) \propto r$, so that $\rho(r) \propto \frac{1}{r^2}$.
Since baryons can interact among themselves they can dissipate their energy and collapse into a disk; dark matter in contrast would not be dissipative and would instead form spherical halos.

Coming to the Milky Way, stellar kinematics allows one to estimate that the halo has a mass $M_{halo} \sim 10^{12}\ M_\odot$ with a local dark matter density of $\rho_0 \sim 0.3$ GeV/cm^3(see [36]; latest measurements favour higher values, such as $\rho_0 \sim 0.4$ GeV/cm^3, see [37]), so that

$$\mathrm{M_{halo}} \sim 4\pi \int_0^{\mathrm{R_{halo}}} \mathrm{dr\ r^2 \rho(r)} \implies \mathrm{R_{halo}} \sim 100\ \mathrm{kpc} \tag{2.2}$$

Another key parameter is the velocity of the dark matter in our galaxy, that is obtained using the virial theorem as $\langle v \rangle \sim \sqrt{\frac{GM_{halo}}{R_{halo}}} \sim 200\ km/s$ (which means the dark matter in galaxies is non relativistic). For more details, see [38].

2.1.2 Bullet Clusters

In 2006 the clash of two galaxies called "Bullet Clusters" was observed (see e.g. [39]); a spectral analysis shows that the clash caused a separation of the individual components of the galaxy clusters, with no collisions between stars.
Through weak-lensing analyses done by the Hubble Space Telescope it has been shown that the gravitational potential's maximum is not where the visible matter density (observed through Chandra-X, as shown in [40]) has its maximum, meaning there must be some matter we can't see through light[34].

In theories without Dark Matter (see as an example Modified Newtonian Dynamics [41]) the lensing would be expected to follow visible matter, but we see that this is not the case.

2.1.3 Cosmic Microwave Background Radiation

Cosmologically, if dark matter existed it must have left its footprint on the CMB; the study of the cosmic microwave background radiation can be used to constrain cosmological parameters such as the abundance of dark energy and of matter.
As we have already said before, the Planck satellite [2] was able to show that Dark Matter makes up approximately 27% of the total energy in the Universe.

Another reason the Modified Newtonian Dynamics seems to be disproved by data is the absence, so far, of a Modified Newtonian Gravity relativistic theory capable of explaining the CMB (see [42]).

2.2 Dark Matter Properties

Now that we have seen the evidences for DM, it's time we start looking at possible candidates.
Before doing this however, we have to specify the properties that all DM candidates must follow in order to be viable choices; we follow for this section the analysis in [7].
The following properties must be satisfied:

- Dark Matter must be dark (or sufficiently weak) with respect to standard model interactions. This requirement comes from the fact that dark matter is not luminous, but there are also other arguments, related to the CMB and the matter power spectrum (where an interaction between DM and SM particles could suppress the power spectrum due to the radiation pressure of the baryons and photons, preventing DM density perturbations from growing);
- Dark Matter must be cold and non-relativistic, otherwise perturbations within an horizon can become washed away due to the motion of DM;
- On large scales DM must be collisionless within its sector, as otherwise there could be a bath of dark radiation, which could interact with a component of the non relativistic dark matter delaying growth of density perturbations and possibly even creating acoustic oscillations;
- Another requirement is that Dark Matter must be stable or close to stability;
- Dark Matter must also preserve results from Big Bang Nucleosynthesis;

2.3 Typical Dark Matter Candidates

Now that we have seen the properties of Dark Matter, we can briefly classify candidates depending on their masses:

- Heavy Dark Matter and Primordial Black Holes: The largest possible mass of a dark matter candidate is generally taken as $10^4 - 10^5$ $M_\odot$ as the least-massive known galaxies have halos of around $10^5 - 10^6$ $M_\odot$ (as explained in [7]). Some models of scalar field Dark Matter can condensate in compact massive objects such as boson stars or axion stars, with masses up to ~ 10 $M_\odot$ (for more informations see [43]).
  Another such example is primordial black holes: these objects form supposedly due to inflationary perturbations (as can be seen in [44]) and their masses that make them hard to produce by accreting stellar remnant BHs(see [45])

- Superheavy Particles: Some particle candidates can be superheavy (with masses ranging from O(10) TeV to $\sim 10^{16}$ g), assuming however they are produced non-thermally as they could have never been in thermal equilibrium with the photon bath (as explained in [7]).

- WIMPs: Weakly Interactive Massive Particles (WIMPs) have been the most studied candidate of dark matter so far. WIMPs have masses that range from 10 GeV up to 10 TeV (see [7]) and have been studied in particular due to them arising from many extensions of the standard model (for example WIMPs can be a neutralino of the minimal supersymmetric standard model, as shown in [46]).

- Light Dark Matter: Candidates with masses ranging from $\sim$ KeV to 10 GeV are called "light", which is a term that generally means they can't be effectively detected by direct detection experiments [7].
  Sub-GeV dark matter is phenomenologically motivated because it could explain the 511 keV excess from the galactic center detected in [47], as explained in [48]. You can see a review on DM models that could explain this excess in [49].
  Another interesting notion to keep in mind is that LHC has still not found clear signs of the Beyond the Standard Model (BSM) physics that motivates the mass range of WIMPs [11], which encourages the study of more candidates.

- Wave Dark Matter: If the mass is lower than 30 eV (down to 10^{-21} eV), DM can behave as a classical wave [50]; one example that has been studied extensively is the QCD axion (see [51]).

2.4 Motivations for Light Dark Matter

Since this thesis is centered around a sub-GeV candidate of DM, we briefly explain the motivations behind light DM.

- Direct Detection experiments such as Xenon-nT[9], PandaX[10] and LZ[52] have weak sensitivities to dark matter with masses below $\sim$ 10 GeV due to their energy thresholds. The lack of detection from these experiments is the first motivation for lighter candidates, which need different methods to be detected.

- In [48] it has been shown that the excess of positrons may be related to the annihilation of dark matter in the inner galactic halo; this excess was first noticed by [47] through an excess in the 511 keV γ-line observed by SPI/INTEGRAL, that was attributed to the positron annihilation in this region.
  They consider the possibility for the decay $\bar{\chi}\chi \to e^+e^-$ with χ being nearly at rest, so that the positrons and electrons will have an energy equal to the dark matter mass, and only the eventual positron's decay will be detectable, producing a 511 keV γ ray.
  They however also show that such an invisible birth is prohibited by the emission of internal bremmstrahlung γ rays unless 1 MeV $< m_\chi <$ 20 MeV , which is a constraint independent on the model considered.
  While this explanation was excluded in [53], in [49] it was found a way to avoid this issue by switching on a coupling with the neutrino and using results from [54, 55].

We also remind that light dark matter could be consistent with bounds from large scale structures and $Lyman-\alpha$ measurements, as can be seen in [56].

Dark matter that couples preferentially to hadrons could be detectable by experiments, with the catch that they must have concrete cosmological histories, as light particles (and light mediators) would contribute to the relativistic degrees of freedom at the time of Big Bang Nucleosynthesis, something we already said should be avoided. For these reasons, we will now extensively talk about one possible candidate of light dark matter, assuming in particular that it can interact with quarks.

Chapter 3

Hadrophilic Dark Matter

3.1 Hadrophilic Dark Matter Model

In this work we look at an Hadrophilic Sub-GeV candidate of Dark Matter with an interaction to the up-quark mediated by a scalar particle. The theoretical framework we consider contains a flavour-specific scalar singlet S with mass m_S coupling primarily with the up quark through a dimension-five operator generated at UV scale M. Notice that the scalar can't couple to more flavours or it would result in flavour changing neutral currents, which are forbidden at tree level and highly suppressed at higher orders (see [57] for a review on experimental searches of FCNC).
Dark matter is taken as a singlet χ, charged under a Z_2 stabilizing symmetry, with mass m_χ as shown in [58]. The relevant terms in the Lagrangian are given as

$$\mathcal{L} \supset i\bar{\chi}(\not{\partial} - m_\chi)\chi + \frac{1}{2}\partial_\mu S \partial^\mu S - \frac{1}{2}{m_S}^2 S^2 - \left(g_\chi S \bar{\chi}_L \chi_L + \frac{c_S}{M} S \bar{Q}_L U_R H_c + h.c.\right) \tag{3.1}$$

which leads, considering $Q_L = (u_L, d_L)$ and $H_c = i\sigma^2 H^*$ (with $H = (h+v)\frac{1}{\sqrt{2}}$ being the Higgs doublet), to

$$\mathcal{L} \supset i\bar{\chi}(\not{\partial} - m_\chi)\chi + \frac{1}{2}\partial_\mu S \partial^\mu S - \frac{1}{2}{m_S}^2 S^2 - (g_\chi S \bar{\chi}_L \chi_L + g_u S \bar{u}_L u_L) \tag{3.2}$$

with $g_u = \frac{c_S v}{\sqrt{2}M}$ and where v=246 GeV is the Higgs vacuum expectation value; we assume c_S will dominate over other dimension-5 operators[58].
Looking at this lagrangian, we see that the spurion c_S (where a spurion is a symmetry breaking parameter that is treated as a fictitious auxiliary field [59]) breaks the flavour symmetry $U(3)^3$ due to the assumption that S couples only with the up quark, which means that, in the quark mass basis, $c_S \propto diag(1,0,0)$.

Due to its interaction with the up-quark mediated by the scalar S, DM will be able to also interact with mesons and nucleons, as we will show in the next section.

3.1.1 Effective Couplings from the Chiral Lagrangian

At low energies, the degrees of freedom of QCD stop being quarks and gluons, but instead become hadrons.
Chiral perturbation theory provides a systematic framework to study strong-interaction at low energies (below $\sim$ 1 GeV, where the spontaneous symmetry breaking of $SU(3)_L \times SU(3)_L \times U(1)_V \to SU(3)_V \times U(1)_V$ gives rise to eight massless Goldstone bosons π). A more detailed explanation can be seen in appendix E, while for a review of the topic see [60].

Since we explicitly want to study mesons decaying to dark matter, this low energy approach seems perfectly fit for our study. If we define $\pi = \pi^a T^a$ (T_a being the Gell-Mann matrices[61]), $f \approx 93$ MeV and $\Sigma = e^{2i\pi/f}$ (see appendix E) we consider, following [20], the relevant terms from the chiral lagrangian

$$\mathcal{L} \supset \frac{f^2}{4} Tr\left[(D_\mu \Sigma)^\dagger D^\mu \Sigma\right]) + \frac{f^2}{4} Tr\left[(\Sigma^\dagger \chi + \chi^\dagger \Sigma)\right] \tag{3.3}$$

where

$$\chi = 2B \begin{pmatrix} m_u + g_u S & 0 & 0 \\ 0 & m_d & 0 \\ 0 & 0 & m_s \end{pmatrix} \tag{3.4}$$

is a spurion containing both the usual quark masses and the effective couplings of S to quarks which transforms as $\chi \to L\chi R^\dagger$ under $SU(3)_L \times SU(3)_R$ [60] (L,R being matrices of $SU(3)_L \times SU(3)_R$) for $g_u \to 0$. B is a dimensionful parameter that can be determined by expanding the chiral lagrangian, resulting in $B \simeq 2.6$ GeV [21, 20].

We parametrize the pion matrix as $\pi = \pi^a t^a + \eta_0 t^0$ (where t^a are the SU(3) generators), which means we can write now

$$\pi = \begin{pmatrix} \frac{1}{\sqrt{2}}\pi^0 + \frac{1}{\sqrt{6}}\eta_8 + \frac{1}{\sqrt{3}}\eta_0 & \pi^+ & K^+ \\ \pi^- & -\frac{1}{\sqrt{2}}\pi^0 + \frac{1}{\sqrt{6}}\eta_8 + \frac{1}{\sqrt{3}}\eta_0 & K^0 \\ K^- & \bar{K}^0 & -\frac{2}{\sqrt{6}}\eta_8 + \frac{1}{\sqrt{3}}\eta_0 \end{pmatrix} \tag{3.5}$$

In this matrix π are the pions, K are the kaons and, once approriately rotated (as we will see later), $\eta_{0,8}$ will give the η and η' mesons.

From the second term on the right hand side of equation 3.3 we see that

$$\mathcal{L} \supset B\frac{f^2}{2}\left(Tr[\Sigma^\dagger(m_q + S g_q)] + h.c.\right) \tag{3.6}$$

with $m_q = diag(m_u, m_d, m_s)$ and $g_q = diag(g_u, 0, 0)$ (as the scalar is only up-philic). We diagonalize the system through the rotation

$$\begin{pmatrix}\eta_8\\ \eta_0\end{pmatrix} = \begin{pmatrix}\cos\theta & \sin\theta\\ -\sin\theta & \cos\theta\end{pmatrix}\begin{pmatrix}\eta\\ \eta'\end{pmatrix} \tag{3.7}$$

where θ is the $\eta - \eta'$ mixing angle, which we take as $\sim -20°$ [62].
For the up-philic scalar S the chiral lagrangian results in the effective interaction

$$\begin{aligned}\mathcal{L} \supset\ & B g_u S\pi^0 \left((\frac{1}{\sqrt{3}}\cos\theta - \frac{2}{\sqrt{3}}\sin\theta)\eta + (\frac{1}{\sqrt{3}}\cos\theta + \frac{2}{\sqrt{3}}\sin\theta)\eta' \right) = \\ &= B g_u S\pi^0 \left(C_\eta \eta + C_{\eta'}\eta'\right)\end{aligned}$$

where $C_{\eta(\eta')} = (\frac{1}{\sqrt{3}}\cos\theta \mp \frac{2}{\sqrt{3}}\sin\theta)$.

Finally, at higher energy chiral perturbation theory is ineffective and the couplings between mesons and S are parametrized through form factors

$$\begin{aligned}\langle M(p)M(p')|m_u\bar{u}u + m_d\bar{d}d|0\rangle &= \Gamma_M(s)\\ \langle M(p)M(p')|m_u\bar{u}u - m_d\bar{d}d|0\rangle &= \Omega_M(s)\end{aligned}$$

where M is the meson we are considering and s is a mandelstam variable given as $s = (p + p')^2$. These factors contain terms that deviate from the chiral lagrangian's results and are generally determined from dispersive analysis and fits to experiments (see e.g. [63]).

3.2 Meson Decays and Interactions with Nucleons

In our study what we really care about is the decay of mesons produced in air showers and, in particular, we are interested in the decays of η and η' mesons. Using the aforementioned effective terms obtained from the Chiral Lagrangian we can obtain straightforwardly (see appendix G) the following Branching Ratios [15]:

$$BR(\eta \to S\pi^0) = \frac{{C_\eta}^2 {g_u}^2 B^2}{16\pi m_\eta \Gamma_\eta} K\left(1; \frac{{m_S}^2}{{m_\eta}^2}; \frac{{m_{\pi^0}}^2}{{m_\eta}^2}\right) \tag{3.8}$$

and

$$BR(\eta' \to S\pi^0) = \frac{{C_{\eta'}}^2 {g_u}^2 B^2}{16\pi m_{\eta'} \Gamma_\eta} K\left(1; \frac{{m_S}^2}{{m_{\eta'}}^2}; \frac{{m_{\pi^0}}^2}{{m_\eta}^2}\right) \tag{3.9}$$

where K is the Kallen Function[64] while $\Gamma_\eta = 1.31$ keV, $\Gamma_{\eta'} = 0.188$ MeV, $m_\eta \approx 548$ MeV, $m_{\eta'} \approx 958$ MeV and $m_{\pi^0} \approx 135$ MeV [65].
These branching ratios are of course not valid for $m_S \geq 420$ MeV for the η meson and $m_S \geq 823$ MeV for the η' meson. In that case, the decay will go directly towards a final state containing a pion and two dark matter fermions $\bar{\chi}\chi$ via an off-shell S.

The DM produced from these decays arrive at detectors and hit nuclei; we will dwelve into this later, but for now this means that we need to study the interactions between nuclei and dark matter. We write the matrix element of the quark bilinear $\bar{q}q$ between nucleons N with mass m_N and initial momentum p_i and final momentum p_f, so that

$$\langle N(p_f)|\bar{q}q|N(p_i)\rangle = \frac{m_N}{m_q} f_q^N F_H(-t)\bar{u_N}u_N \tag{3.10}$$

where F_H is a form factor we will write later and $f_q^N = \frac{\langle N|m_q\bar{q}q|N\rangle}{m_N}$ at the leading order in the expansion for small q^2. In particular, given the lagrangian containing the effective interactions

$$\mathcal{L} \supset y_{Spp} S\bar{p}p + y_{Snn} S\bar{n}n \tag{3.11}$$

we can see that

$$y_{Spp} = g_u\langle p|\bar{u}u|p\rangle = g_u\frac{f_{Tu}^p m_p}{m_u} \tag{3.12}$$

and

$$y_{Snn} = g_u\langle n|\bar{u}u|n\rangle = g_u\frac{f_{Tu}^n m_p}{m_u} \tag{3.13}$$

where $f_{Tu}^p = 0.014$ and $f_{Tu}^n = 0.012$[66]. If the energy is not enough to resolve the nuclear structure, we can see that these coefficients come into play in

$$i\mathcal{M} = i\frac{g_\chi(y_{Spp}Z + y_{Snn}(A-Z))}{(p^2 - m_S^2)} F_H(-t)\bar{\chi}\chi\bar{N}N \tag{3.14}$$

which is the matrix element associated to the scattering $\chi N \to \chi N$.
From this we can compute the cross-section of the interaction $\chi N \to \chi N$ between dark matter and nuclei, obtaining:

$$\frac{d\sigma}{dT} = \frac{1}{K_{max}}\frac{{g_\chi}^2(Zy_{spp} + (A-Z)y_{snn})^2}{16\pi s}\frac{(-t + 4{m_\chi}^2)(-t + 4{m_N}^2)}{({m_S}^2 - t)^2} F_H^2(-t)\Theta(K - K_{max}) \tag{3.15}$$

where A, Z and m_N are respectively the nucleon number, atomic number and mass of the nucleus we consider. T is the initial kinetic energy of the recoiling particle (either DM or the nucleus), s is a Mandelstan variable given as $s = (P_1 + P_2)^2$ (with P_1 and P_2 being the initial four-momenta of DM and the nucleus), K is the

final kinetic energy of the recoiled particle while K_{max} is given by reference [67]. For nuclei and nucleons being hit in detectors we consider the nucleus/nucleon's frame of reference, where the Mandelstan variable $t = 2m_N T_N$ (T_N is the recoil energy given to the nucleus/nucleon by DM), obtaining

$$\frac{d\sigma}{dT_N} = \frac{{g_\chi}^2 (Z y_{spp} + (A-Z) y_{snn})^2}{8\pi} \frac{(T_N + 2{m_N}^2)(m_N T_N + 2{m_\chi}^2)}{(m_S{}^2 + 2m_N T_N)^2} {F_H}^2 (2m_N T_N) \Theta(T_{N,max} - T_N) \tag{3.16}$$

in the form seen in [15].

The form Factor $F_H(-t)$ is taken from [22] as:

$$F_H(q^2) = \left(\frac{3 j_1(qR_1)}{qR_1} \right) e^{-q^2 s^2/2} \tag{3.17}$$

where $j_1 = \frac{\sin x}{x^2} - \frac{\cos x}{x}$ is a spherical Bessel function of the first kind and

$$R_1 = \sqrt{c^2 + \frac{7}{3}\pi^2 a^2 - 5s^2} \tag{3.18}$$

with $c \simeq (1.23 A^1/3 - 0.60) fm$, $a \simeq 0.52 fm$ and $s \simeq 0.9 fm$.
This form factor is obtained by fitting directly to experimental data covering a range of nuclei with $A \geq 9$ [68]; for hydrogen we are going to use the form factor from [69] given as

$$F_H(q^2) = \frac{1}{(1 + (q/\Lambda)^2)^2} \tag{3.19}$$

where $\Lambda = 770$ MeV.

3.3 Cosmology of The Model

A key aspect of any DM candidate is that it must be cosmologically viable.
In this section we show the cosmological impact of hadrophilic sub-GeV DM, throwing the basics concept that we will use later to derive relevant limits from cosmology.

3.3.1 Brief Review of Particle Cosmology

Now we review the cosmology of particles in the early universe, for more informations see [38, 70]. For a review specifically on Dark Matter in cosmology, see [71]. The universe was originally in thermal equilibrium; the various particles inhabiting the early universe were in a thermal bath, in equilibrium with each other.

Due to the expansion of the Universe, the density of particles at thermal equilibrium would decrease in time, meaning the possibility of reactions happening would decrease too as a consequence. There is then a time for each particle when they "freeze out" or "decouple" from the thermal bath. This happens when the interaction rate falls behind the expansion rate of the universe.
In general we can write the interaction rate as

$$\Gamma = n\langle\sigma v\rangle \tag{3.20}$$

where n is the equilibrium number density and it depends on whether we have a relativistic or non relativistic species:

$$\begin{cases} n = g\left(\frac{mT}{2\pi}\right)^{3/2} exp(-(m-\mu)/T), m \gg T \\ n = \frac{\zeta(3)}{\pi^2} gT^3, m \ll T \end{cases} \tag{3.21}$$

where μ is the chemical potential, g is the degeneracy factor and, if the relativistic particle is a fermion, there is an additional $3/4$ in front of g.
Freeze-out will happen when $\Gamma \sim H$, where H is the Hubble parameter. For a radiation-dominated epoch, $H \sim \sqrt{\rho}/M_{pl}$ (with $M_{pl} \approx 2.4 \times 10^{18}$) and it scales as

$$H \sim T^2/M_{pl} \tag{3.22}$$

After obtaining the freeze-out temperature (by comparing $\Gamma \sim H$) we use the Boltzmann Equation

$$\dot{n}_\chi + 3Hn_\chi = -\langle\sigma v\rangle({n_\chi}^2 - (n_\chi^{eq})^2)^2 \tag{3.23}$$

which we simplify by using $Y = n_\chi/s$ and $x = m_\chi/T$ (with Y being the actual number of particles per comoving volume, s being the entropy density) obtaining

$$\frac{dY}{dx} = -\frac{xs\langle\sigma v\rangle}{H(m)}(Y^2 - {Y_{eq}}^2) \tag{3.24}$$

where the "eq" means at equilibrium.
If the relics decouples while hot ($x \ll 3$), we will see that

$$Y_{eq} = \frac{45\xi(3)}{2\pi^4}\frac{g_{eff}}{g_{*s}} \tag{3.25}$$

and if cold ($x \gg 3$) then

$$Y_{eq} = \frac{45}{2\pi^4}\left(\frac{\pi}{8}\right)^{1/2}\frac{g}{g_{*s}}x^{3/2}e^{-x} \tag{3.26}$$

where $g_{eff} = g$ if bosons and $g_{eff} = 3g/4$ for fermions while $g_{*s} = \sum_B g_B \left(\frac{T_B}{T_\gamma}\right)^3 + \frac{3}{4}\sum_F g_F \left(\frac{T_F}{T_\gamma}\right)^3$ (where "B" stands for bosons, "F" stands for fermions and T_γ is the temperature of the plasma).
For the current abundance of stable species we can see that

- For hot relics the freeze out occurs when the particle is relativistic and Y_{eq} is not changing in time, in particular we can see that $\frac{dY}{dx} \simeq 0$ and so $Y_\infty = Y_{eq}(x_f)$ (where x_f is the value of x at freeze-out and Y_∞ is the actual number of particles per comoving volume now).
  We can then see that the contribution to the energy density of this particle ψ will be given as

  $$\Omega_\psi h^2 = 7.83 \times 10^{-2}(g_{eff}/g_{*s}(x_f))(m/eV) \tag{3.27}$$

  with $\Omega_\psi = \frac{\rho_\psi}{\rho_{crit}}$ (with $\rho_{crit} = 3H_0^2/8\pi G$ and H_0 being the Hubble parameter today) and $h = H_0$ in units of 100 $km/s/Mpc$, so that $h = 0.68$[2].

  Since we know that $\Omega_0 h^2 \leq 1$ we can put a bound to the mass of ψ given as $m \leq 12.8(g_{*s}/g_{eff})$ eV; notice that this bound depends on the value of g_{*s} at the freeze-out, which means that, if a particles decouples very early when this value is large, its present number density will be smaller.

- For cold relics Y_{eq} instead decreases exponentially with x; the annihilation cross-section can be parametrized as $\sigma_A|v| \sim v^p$ with $\langle v\rangle \sim T^{1/2}$ so that $\langle\sigma_A|v|\rangle \sim T^n$ with $n = 0$ for s-wave annihilation and n=1 for p-wave annihilation.
  For this reason we can parametrize

  $$\langle\sigma_A|v|\rangle = \sigma_0(T/m)^n = \sigma_0 x^{-n} \tag{3.28}$$

  so that $dY/dx = -\lambda x^{-n-2}(Y^2 - Y_{eq}^2)$ with $\lambda = \left(\frac{x\langle\sigma_A|v|\rangle s}{H(m)}\right)$ and $Y_{eq} = 0.145(g/g_{*s})x^{3/2}e^{-x}$.
  This equation can be solved approximately, but we just write the solution, which is

  $$Y_\infty = \frac{n+1}{\lambda} x_f^{n+1} \tag{3.29}$$

  We now obtain the energy density given as

  $$\Omega_\psi h^2 = 1.07 \times 10^9 \frac{(n+1)x_f^{n+1}\mathrm{GeV}^{-1}}{(g_{*s}/g_*^{1/2})M_{pl}\sigma_0} \tag{3.30}$$

  The smaller the annihilation cross section is, the greater will be the relic abundance [70].

3.3.2 Cosmology of the Scalar Mediator

At the moment of BBN the mediator S can contribute to the number of relativistic degrees of freedom, which is constrained by the primordial element abundance. Since S can also possibly decay into photons for $m_S > 2m_\pi$ it can also affect the baryon-to-photon ratio, which can decrease the deuterium abundance.
Following [20] it is shown that if the scalar stays at thermal equilibrium until kinetic decoupling $m_S > 20$ MeV is a required condition to prevent changes to the BBN results. If the mediator decouples before the BBN, but still affect the baryon-to-photon ratio, the condition $g_u > (2 \times 10^{-8})(m_S/\text{GeV})^{-3/2}$ must hold.
We can roughly obtain these limits by making the following analysis: before the QCD phase transition, the scalar production is driven by $\bar{u}u \to S$, $\bar{u}u \to Sg$ and $ug \to uS$. For small m_S, the production rate of S is given as $\Gamma_S \sim g_u^2 T$.
S will reach thermal equilibrium as soon as $\Gamma \sim H$; by requiring the freeze-out temperature to be greater than the BBN temperature ([20] considers $T > 1$ GeV), we can then obtain a limit from $T \sim M_{pl} g u^2$.
It must be noticed that these conditions won't affect our results. In particular we will be mostly interested in $m_S > 2m_\pi \approx 270$ MeV, where S will decay too fast to produce changes to the BBN.

3.3.3 Cosmology of Dark Matter

If $m_\chi < m_S$ (the case we consider), χ will annihilate to SM particles.
The DM's annihilation rate will depend on the decay rate Γ_S for the mediator S as

$$\langle \sigma v_{rel} \rangle_{\bar{\chi}\chi \to S\bar{M}SM} = \frac{g_\chi^2 m_\chi v_{rel}^2 \Gamma_S|_{m_S=2m_\chi}}{2\left((ms^2 - 4m_\chi^2)^2 + m_S^2 \Gamma_S^2\right)} \tag{3.31}$$

where $\Gamma_S|_{m_S=2m_\chi}$ is the decay width of S when $m_S = 2m_\chi$.
Now either $m_S \gg \Lambda_{QCD}$ and $S \to \bar{u}u$ will lead to $\Gamma_S = 3g_u^2 m_S/8\pi$ or we need to consider hadronic effects.

I briefly introduce the fact that, if we considered a mediator S coupled to a more massive quark instead of the up quark (like the top quark or an even more massive quark ψ), the interactions between the mediator and the nucleons would be greatly weakened; this may result in a situation where the interactions between dark matter and the standard model bath are so weak that equilibrium is never achieved, leading to a production mechanism called "freeze-in"[72]. See [73] for an example in a model similar to our.

3.4 Existing Limits

We now review the phenomenology of sub-GeV hadrophilic DM, in particular reviewing existing limits from the literature.

3.4.1 Limits from Cosmology

We start with the limits coming directly from cosmology, a topic we already explored. For more informations on these limits, you can see [23, 20].
Bounds from BBN have already been discussed when it comes to the scalar mediator. For the dark matter candidate, based on the results of section 4.1 of [23], we impose $m_\chi > 10\ MeV$. This condition can be relaxed if we switch on a coupling of the mediator to neutrinos.

Another issue is the DM abundance: after the QCD phase transition χ will have to decay into pions otherwise it won't reach the correct dark matter abundance, which requires $m_\chi > m_\pi$ to happen.
For masses m_χ smaller than m_π dark matter can still reach the correct abundance via thermal freeze-out by adding a small coupling to electrons or neutrinos. Furthermore if the dark matter annihilation cross section is larger than the thermal one (for example if m_χ is larger enough than m_π or if it is coupled to neutrinos) the symmetric dark matter component annihilate away, leaving only a possible initial asymmetric component and allowing to reproduce the measured DM abundance without altering the phenomenology that we will discuss in this thesis.

For the regions of the parameter space allowed and considered in this thesis, the DM annihilations into mediators (if kinematically allowed), mesons and quarks are all p-wave suppressed, so no constraint would come from the CMB [23].

3.4.2 Limits from Colliders

Collider searches have no lower limit to the DM masses they are sensitive to and for this reason they can efficiently constrain sub-GeV dark matter.
One technique involves the comparison of the observed mono-jet events to the number of events expected from standard model backgrounds; from this one can derive limits on the suppression scale Λ of the effective dark matter couplings as a function of the dark matter mass m_χ, which can be then converted in constraints on the dark matter-nucleon scattering cross section [74].

Dark Matter pairs can be produced at colliders through $\bar{u}u \to Sg \to \bar{\chi}\chi g$ where S can be produced on-shell or off-shell, depending on the mass. By simulating the monojets [23] finds that, for m_S=1 GeV and m_χ varying between 10 MeV and 10 GeV, $g_u g_\chi \lesssim 0.06$.

They also consider the possibility that a coupling to the top quark would induce at one-loop a bSs (where b is the bottom quark and s the strange quark) vertex, constrained by $B \to KS \to$invisible; constraints on hypothetical couplings to charm and bottom would come respectively from $Y \to S\gamma \to$invisible and $J/\psi \to S\gamma \to$invisible.

3.4.3 Limits from Astrophysics

By considering the cooling of Supernova Remnants such as SN 1987 A we can obtain limits on the coupling with nucleons (as is generally done for axions for example, see [75]).
For an up-philic scalar we would have a bremsstrahlung process $NN \to NN + S$ happening in the core where one of the nucleons takes the role of a spectator, which has the purpose of allowing the process to happen kinematically.
Following [76] we can see that the differential cross section will be

$$d\sigma[NN \to NN + S] \approx d\sigma[NN \to NN] \frac{d^3 k_S}{(2\pi)^3 2E_S} \beta_f y_{SNN}^2 \times \\ \times \left(\frac{2E_S^3 - m_S^2 E_S - 2m_S((\boldsymbol{k_s} \cdot \boldsymbol{\beta_i})^2 - (\boldsymbol{k_s} \cdot \boldsymbol{\beta_f})^2)}{m_N E_S^3} \right)^2$$

where $\beta_{i,f}$ are the non relativistic velocities of an initial-state and a final-state nucleon, y_{SNN} is the previously written coupling between S and nucleons (in this case neutrons) and the energy is $E_S = m_N(\beta_i^2 - \beta_f^2)$, with 3-momentum k_S associated.
The thermally averaged energy loss is

$$Q_S(T) = \int_{\sqrt{m_S/m_N}}^{\infty} d\beta_i \beta_i f_N(T, \beta_i) \int d\sigma[NN \to NN + S] E_S n_N^2 \qquad (3.32)$$

where $n_N \approx 1.8 \times 10^{33}$ cm^{-3} [20] is the nucleon number density in the core while f_N is the Maxwellian nucleon distribution function.
By comparing $Q_S(T)$ to the observational bound [77] $Q_S \lesssim 3 \times 10^{33}$ erg cm^{-3} s^{-1} and using the temperature of the Neutron Stars $T \approx 30$ MeV and $d\sigma[NN \to NN] \approx 2.5 \times 10^{-26}\, cm^2$ (see [76]), [20] finds a limit for y_{SNN} which can translate to a limit for g_u.
Simplifying the core plasma as only made of neutrons due to the small difference

between f_{Tu}^n and f_{Tu}^p one finds that if g_u is sufficiently large, the scalars emitted through bremsstrahlung will be trapped within the supernova core unable to escape, occurring through the absorption $NN + S \to NN$ (or the decay of S in dark matter or in pions if the dark matter decay channel is not available).
We can evaluate the absorption through the effective mean opacity given as

$$k_S = \frac{\frac{8}{15}\pi^4 T^3}{m_N \int_{m_S}^{\infty} dE_S E_S^3 (1 - m_S^2/E_S^2)\sigma_{abs}^{-1} \frac{\partial}{\partial T}(e^{E_S/T} - 1)^{-1}} \tag{3.33}$$

which we then compare to the neutrino opacity (trapping happens when $k_S > k_\nu$).

If the decay width of $S \to \bar{\chi}\chi$ is sufficiently large (large enough so that λ_S, the decay width of the scalar mediator, is smaller than the size of the SN core) this constraint is governed by $\chi + N$ scattering rather than the absorption of S; if we assume a single scattering is sufficient to trap a dark matter particle in the core we can then compare the associated opacity k_χ to the neutrino opacity, given as $k_\nu \approx 8 \times 10^{-17}\ cm^2/g$ and constraining $g_u g_\chi$.

The resulting constraint[20] excludes the region with $m_S < 10^{-3}$ GeV and $10^{-10} < g_u < 10^{-9}$, where $g_\chi = 1$ and $m_S = 3m_\chi$.

3.4.4 Limits from Direct Detection

For classical wimps, which are assumed to have a speed consistent with the solar system's speed (around 220 km/s), the collision with a nucleus with a negligible initial speed can lead to a final nucleus kinetic energy given as

$$E_R = \frac{q^2}{2m_N} \tag{3.34}$$

where q is the momentum transfer given as **q=p-p'** (p and p' are the initial and final momentum of the WIMP). We can see that for an elastic non-relativistic scattering

$$\begin{cases} \boldsymbol{p} = \boldsymbol{p'} + \boldsymbol{q} \\ \frac{p^2}{2m_\chi} = \frac{q^2}{2m_\chi} + \frac{p^2}{2m_N} \end{cases} \tag{3.35}$$

will lead to

$$E_R^{MAX} = \frac{1}{2} m_\chi v_\chi^2 \frac{m_\chi m_N}{(m_N + m_\chi)^2} = \frac{1}{2} v_\chi^2 \frac{\mu^2}{m_N} \tag{3.36}$$

where $\mu = \frac{m_\chi m_N}{m_\chi + m_N}$ is the reduced mass and v_χ is the DM's velocity in the laboratory frame of reference [78].
In the center of mass frame of reference the velocity of DM will be $v'_\chi = v_\chi + v$, with $v = m_\chi v_\chi/(m_\chi + m_N)$. For an elastic scattering the DM will change direction

after the collision, with $|\boldsymbol{p}| = |\boldsymbol{p'}|$. For $\boldsymbol{q} = \boldsymbol{p'} - \boldsymbol{p}$ we see that

$$\frac{q^2}{2} = p^2 - \boldsymbol{p} \cdot \boldsymbol{p'} = p^2(1 - \cos\theta) = \mu^2 v_\chi^2 (1 - \cos\theta) \tag{3.37}$$

where $p = |\boldsymbol{p}| = m_\chi v'_\chi = \mu v_\chi$ and θ is the angle between the initial and final momenta of the dark matter in the center of mass frame of reference. Using $E_R = q^2/2m_N$ (with E_R taking the value of the lower energy threshold of our detector in this case) can then obtain the minimum velocity required to have a recoil

$$v_{min} = \sqrt{\frac{m_N E_R}{2\mu^2}} = \frac{q}{2\mu} \tag{3.38}$$

with $m_\chi << m_N$. For detectors such as Xenon1T that use heavy nuclei like Xenon, the energy threshold of a few KeV makes the sensitivity degrade for $m_\chi \lesssim 10$ GeV, but makes them optimal when $m_\chi \sim 100$ GeV[38].

Combining the results from Xenon1T ([9, 79]), CRESST-III [80] and DarkSide50 [81] one can see the strongest constraints from direct detection. With CRESST-III we observe limits even for $m_\chi \simeq 160$ MeV, as this experiment operated 10 cryogenic detector modules with solid $CaWO_4$ crystals optimized for low energy thresholds.

Chapter 4

Breef Review of Air Showers and Cosmic Rays

When high energy cosmic rays strike the Earth's atmosphere they can start a cascade of secondary particles, which can interact with the atmosphere and decay, resulting in what is called an "air shower".
Air showers have been in the past a key factor in the discovery of new particles, starting with the muon in 1937[17, 19], initially mistaken for the pion, that was actually discovered in 1947 [18].
Hadrons were discovered very fast from this moment, with the discovery of the kaons happening in the same year as the discovery of the pion [82] followed by the discovery of the Λ baryon a few years after. For a review on the topic, see e.g. [83].

In this chapter we will discuss cosmic rays (CR) and air showers briefly, explaining in particular how hadronic showers work. We are interested in the idea that, just like historically the discovery of hadrons happened through cosmic rays interacting in the atmosphere, we may be able to do the same for dark matter.

4.1 Cosmic Rays

Primary cosmic rays are all the high-energy stable particles like protons, fully ionized nuclei and electrons that continually arrives at Earth and hit the atmosphere. The vast majority of high-energy CRs are protons, with only 10% being Helium and 1% being neutrons or other heavier nuclei. Together these all accounts for 99% of the cosmic rays, while the remaining 1% are electrons and photons (with neutrinos estimated to be comparable to photons) [24].

For these cosmic rays we can define their flux per unit area A and time T as

$$\phi(E) = \frac{\mathrm{d(N/(AT))}}{\mathrm{d\Omega dE}} \frac{\text{particles}}{\mathrm{cm^2\ sr\ s\ GeV}} \tag{4.1}$$

where N/(AT) is the number of particles per units of area and time, $d\Omega$ is the differential solid angle and dE is the given energy interval[25].
For a more detailed introduction to cosmic rays, see [84].

4.1.1 Energy Spectrum of Cosmic Rays

The distribution of energy of cosmic rays is described by a power law E^{-p} where p is between 2.7 and 3.3, with two clear changes in slope around " around $5{\times}10^{15}$ eV, and the "ankle" around 5×10^{18} eV. A strong suppression of the flux can be seen at 5×10^{19} eV, caused by the destructive interaction of high-energy particles with the Cosmic Microwave Background Radiation (CMB) [24]. The low energy region is dominated by cosmic rays from the sun, while the higher energies (above $\sim$ 1000 TeV) are dominated by astrophysical sources from our galaxy.
At 5×10^{15} eV there is a change in slope often referred to as the "knee", with Extragalactic sources supposedly being the origin of these high energy CRs.
For even higher energies, at 5×10^{18} eV, there is once again a change in slope, that is called the "ankle", where the flux becomes less steep.

In figure 4.1 (that is taken from reference [85]) all the features of the cosmic ray spectrum are shown.

In figure 4.2 the flux of protons and helium is obtained following the approach presented in [23]: for energies lower than 100 MeV we took the fluxes from [86], for energies between 100 MeV and 50 GeV we considered [87] and finally for energies over 50 GeV we consider [88].

4.1.2 Acceleration of Cosmic Rays

To better understand how CRs can be so energetic, we now review the mechanisms at the core of their acceleration. We follow for this analysis [24].

Fermi Mechanisms

We first start this section by explaining the mechanisms that can accelerate cosmic rays. For more informations on this mechanisms, see [89].
Let's consider a charged particle (like a proton) scattering off against a moving boundary, for example a gas cloud. The moving cloud has a speed $\beta = V/c$ (and associated Lorenz factor γ) while the proton is moving with an incident angle θ_1 and, after bouncing, an angle θ_2 with respect to the velocity of the cloud.

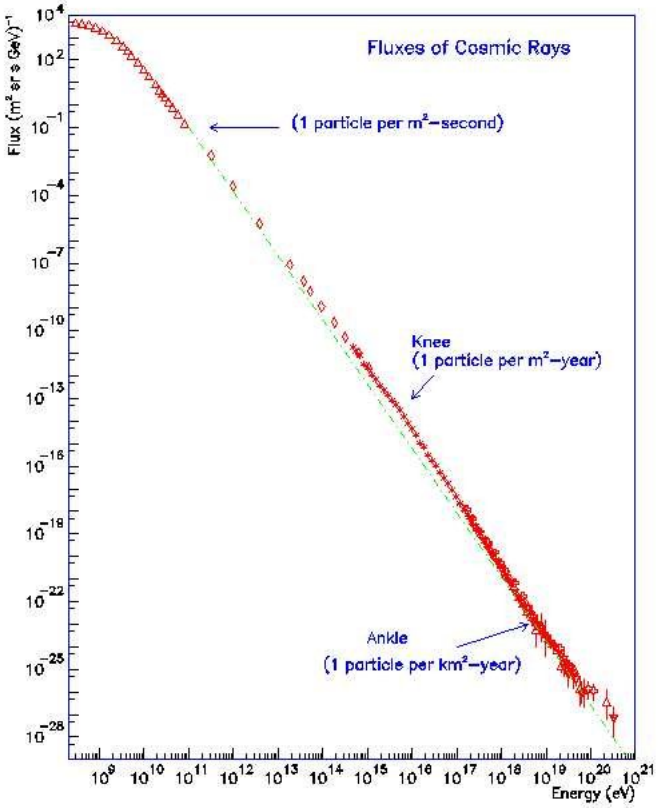

Figure 4.1 All cosmic rays energy spectrum. Picture from [85]

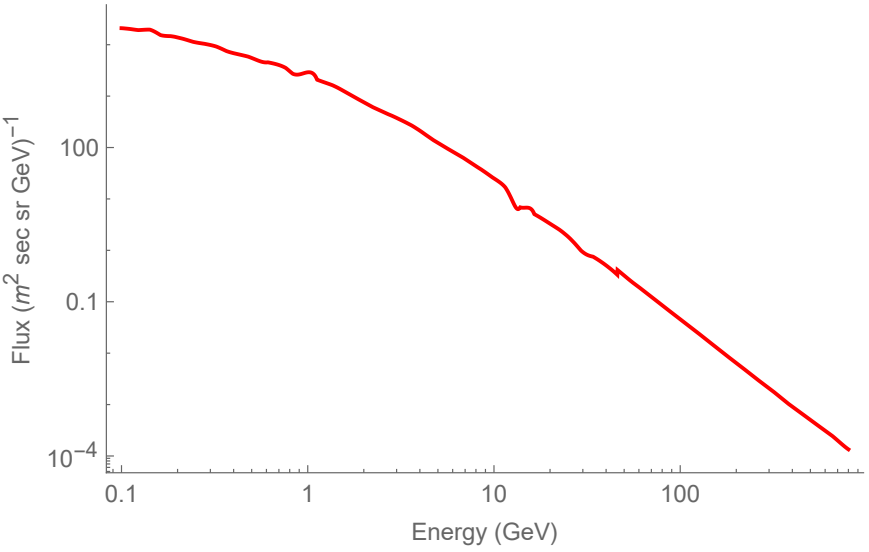

Figure 4.2 Flux of Protons plus Helium, presented from [23]

The starting energy of the proton in the frame of reference of the cloud will be given as

$$E_1^* = E_1\gamma(1 - \beta\cos\theta_1) \tag{4.2}$$

which is equal to the energy after the collision (as the cloud is much more massive), given as $E_2^* = E_1^*$. In the laboratory frame $E_2 = E_2^*\gamma(1 + \beta\cos\theta_2^*)$ which means

$$\frac{\Delta E}{E} = \frac{E_2 - E_1}{E_1} = \gamma^2(1 - \beta\cos\theta_1 + \beta\cos\theta_2 - \beta^2\cos\theta_1\cos\theta_2) - 1 \tag{4.3}$$

The proton will scatter multiple times inside the cloud, so that $\langle\cos\theta_2\rangle = 0$. However, the probability of a scattering between the proton and the cloud happening is proportional to their relative velocity (with the proton having a velocity v in the laboratory frame, with v being close to c for high-energy cosmic rays) as $P \propto (v - V\cos\theta_1) \propto (1 - \beta\cos\theta_1)$ which means

$$\langle\cos\theta_1\rangle = \frac{\int_{-1}^{+1}\cos\theta_1(1 - \beta\cos\theta_1)d\cos\theta_1}{\int_{-1}^{+1}(1 - \beta\cos\theta_1)d\cos\theta_1} \simeq -\frac{\beta}{3} \tag{4.4}$$

so that

$$\langle\frac{\Delta E}{E}\rangle \simeq \frac{4}{3}\beta^2 \tag{4.5}$$

This is the second order Fermi mechanism, which is generally not too effective as the gain in velocity is proportional to β^2 with $\beta \sim 10^{-4}$.

Let's now consider a shockwave (obtained for example when a supernova ejects a sphere of hot gas faster than the local speed of sound into the interstellar medium) that is moving towards some gas cloud. In the reference frame of the shock front, the gas cloud moves towards the shockwave with a velocity $\boldsymbol{u_u}$ while the shocked gas moves away with velocity $\boldsymbol{u_d}$.
If we consider a particle moving back and forth between the shocked gas and the medium, we will see that the system is dynamically equivalent to a pair of mirrors bouncing a ball between each other with a relative velocity given as $V = |\boldsymbol{u_u}| - |\boldsymbol{u_d}|$, where in a supersonic shock in general $|\boldsymbol{u_u}| \sim 4|\boldsymbol{u_d}|$.
If we call θ the angle between the direction of the shockwave and the direction of the moving proton, seeing that

$$\frac{\Delta E}{E} \simeq -2\beta\cos\theta \tag{4.6}$$

with $-1 < \cos\theta < 0$ with a probability of crossing the wave front proportional to $-\cos\theta$, so that now $\langle\cos\theta\rangle \simeq \frac{\int_{-1}^{0} -\cos\theta^2 d\cos\theta}{\int_{-1}^{0} -\cos\theta d\cos\theta} = -\frac{2}{3}$ and now

$$\langle\frac{\Delta E}{E}\rangle \simeq \frac{4}{3}\beta \equiv \epsilon \tag{4.7}$$

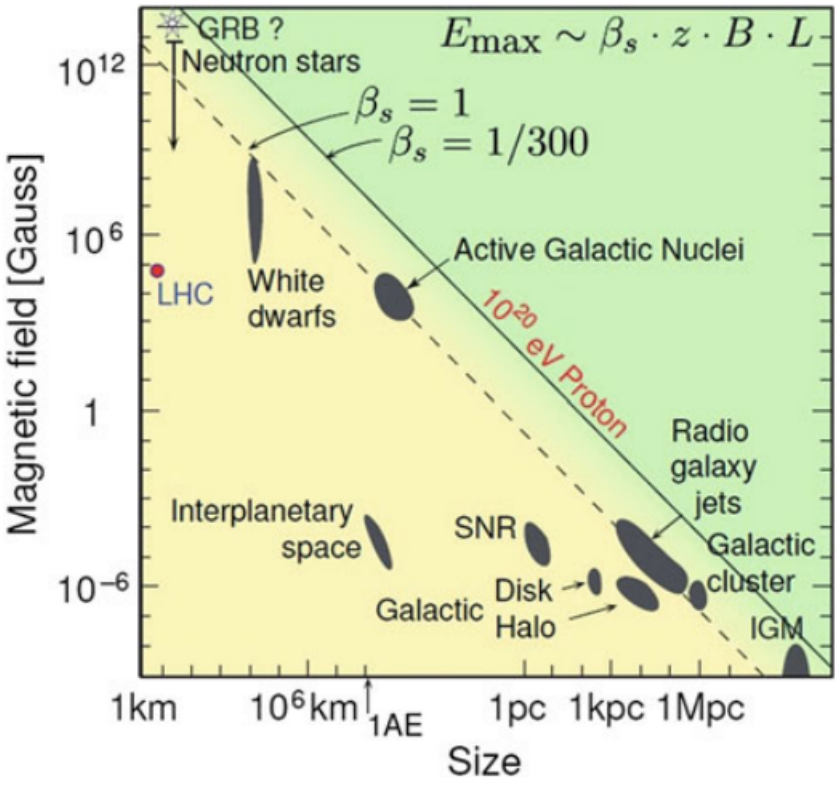

Figure 4.3 The so called "Hillas Plot", showing the comparison between magnetic field and size for several astrophysical objects. From http://astro.uni-wuppertal.de/~kampert

This is called a first order Fermi mechanism. For n cycles we will have that $E = E_0(1+\epsilon)^n$, predicting that the energy spectrum will be a power law with an almost constant index as observed above. [24]

Acceleration Sites

Since we have explained how CRs are accelerated, it's only natural to also look at possible sites where this acceleration could take place. You can see references [24, 90] for more informations.
In order to effectively accelerate particles, a sources must have at least a size R of the order of the particle Larmor Radius, $r_L = \frac{p}{ZeB}$ (with Z being the atomic number of the CR, B the magnetic field, e the charge of the electron and p the momentum of the CR).

This relation $R \sim r_L$ can be rewritten as

$$\frac{E}{1PeV} \simeq \frac{B}{1\mu G} \times \frac{R}{1pc} \tag{4.8}$$

where E is the energy of the particle.
Notice that static magnetic fields can't accelerate particles, while static electric fields would get neutralized very fast. For varying magnetic fields however we see that they can induce variable electric fields that can accelerate cosmic rays.
Possible acceleration sites that satisfy these conditions are listed here:

- Supernova Remnants are the structure left after the explosion of a star at the end of its life cycle, very often resulting in a Neutron Star (NS). Due to the conservation of angular momentum, NSs (with a radius of approximately only 20-30 km) can have a very short period of rotation, while the magnetic field is increased due to the gravitational collapse. For a typical value of $B_{STAR} \sim 1\ kG$ the magnetic field of the NS can be $10^{12}\ G$.

- The shockwave from a supernova can heat the interstellar material it encounters, leading to a magnetic field of about $B \sim 10\ \mu G$ up to 1 mG.

- Pulsars slowing down their rotation can produce a relativistic magnetized particle wind, which radiates synchrotron photons which might possibly undergo Inverse-Compton scattering

- Around 10% of Active Galactic Nuclei exhibit relativistic jets due to the accretion of the black hole's disk. These objects emit photons over a wide range of wavelengths from γ to radio and cosmic rays up to much higher energies

4.2 Air Showers

The Earth is constantly hit by high energy cosmic rays. When an hadronic particle enters the atmosphere it will interact with a nucleus, producing a shower of secondary particles.
Showers can in general be of electromagnetic nature or hadronic nature. For more informations on air showers, see [91].
To know more about air showers simulations (something that is very important for this this work) see reference [92].
For this section on air showers we follow mainly [25].

4.2.1 Atmosphere Model

The flux of any standard model particle propagating through the atmosphere is a function of the so called "atmospheric depth", given as the integral in altitude of the density above the observation level h:

$$X_v = \int_h^\infty \rho(h')dh' \tag{4.9}$$

The pressure can be written as $p = \frac{mg}{S} = \frac{g}{S}\int_h^\infty \rho(h')Sdh' = g\int_h^\infty \rho(h')dh'$ (with m being the mass of the column of atmosphere above h), so that

$$p = gX_v \tag{4.10}$$

where $\rho = -\frac{dX_v}{dh}$ (the minus sign represents that the density decreases as h increases).
If the atmosphere is a perfect gas, we can use its equation of state $pV = Nk_BT$, rewriting it so that $p = \rho\frac{k_BT}{M}$ and finally obtaining

$$\rho = \frac{Mp}{k_BT} \tag{4.11}$$

where k_B is the Boltzmann constant, M is the molecular mass of air (which is made mainly of molecular nitrogen, 78%, and oxygen, 21%, so that $\langle A\rangle \simeq 14.5$ and $M = 2A_{atm} \times m_p = 4.8 \times 10^{-23} g$[25]).
We can write the temperature as a function of the atmospheric depth, obtaining

$$T = -\frac{M}{k_B}\frac{gX_v}{dX_v/dh} \tag{4.12}$$

While we know the temperature slowly decreases with height in the atmosphere, we can assume it as constant as a first approximation, so that

$$X_v = X_v^{atm}e^{-h/h_0} \tag{4.13}$$

where $X_v^{atm} = 1030\ g\ cm^{-2}$ and $h_0 = k_BT/Mg$; assuming we are at the surface of the Earth (where $T \simeq 290$ K) we can see that $h_0 \simeq 8.4$ km.

We can also define a new quantity, called the "slant depth", which is given as

$$X(l,\theta) = \int_l^\infty \rho(h(l,\theta))dh \tag{4.14}$$

where

$$h(l,\theta) = \sqrt{R_{EARTH}^2 + 2lR_{EARTH}\cos\theta + l^2} - R_{EARTH} \tag{4.15}$$

So that, for $\theta < 60^\circ$, we can see that $X \simeq \frac{X_v}{\cos\theta}$ and $\rho = \frac{X_v}{h_0} \simeq \frac{X\cos\theta}{h_0}$; $R_{EARTH} \simeq 6370\ km$ is the radius of the earth [25][93].

4.2.2 Hadronic Cascades

Protons, neutrons and heavier nuclei can initiate hadronic showers by hitting nuclei in the atmosphere. The number of charged hadrons increases as $n_{ch} \propto E_0^{0.2}$ (as found from $\bar{p}p$ and pp data in [94]), where E_0 is the laboratory energy of the cosmic ray.

The produced $n_h = \frac{3}{2} n_{ch}$ of total hadrons, which are mainly pions[95], carry a fraction k of the initial energy that is called "inelasticity" and is generally taken as $k \simeq 0.7$ for the initial primary cosmic ray.
Inelasticity takes into account the fact that a significant fraction of the energy is taken away by a single massive leading particle, such as

$$k = \frac{E_0 - E'}{E_0 + M_T} \tag{4.16}$$

where M_T is the mass of the target nucleon and E' is the residual energy of the nucleon after the collision. The energy E' is then used by the leading particle to interact again and generate another shower.
After n interactions, the leading particle will have a fraction $(1-k)^n$ of the initial energy E_0. Interactions will continue until the hadron energy falls behind a certain interaction threshold.

Let's consider now a particle P with a decay length dP' (which is the decay length in P's frame of reference). We can define the decay length considering the density of the medium ρ as

$$dP_\rho = dP' \cdot \rho \tag{4.17}$$

Notice that this is not a real length, but it has the units of a column depth.
We also consider the interaction length λ_P such that a particle P will either decay or interact depending on whether dP_ρ is bigger than λ_P (which means it will interact) or not (which means it will just decay). For pions (the main hadronic product), $\lambda_\pi \simeq 120\ g\ \mathrm{cm}^{-2}$.
As a first approximation we follow [96], saying that the particle P interacts if the energy is above a threshold E_{dec} and decays otherwise. We can derive this energy by requiring that

$$\lambda_P = dP' \cdot \rho = \left(\frac{E_{dec}}{m_P c^2} \right) c\tau_P \cdot \rho \tag{4.18}$$

where τ_P is the mean lifetime of particle P. Using $\rho \sim 10^{-3}$ g cm^{-3}, equation 4.18 leads to $E_\pi \simeq 20$ GeV for pions.

Part of the energy is transfered to the electromagnetic component of the shower and we can see that the fraction remaining to the hadrons after n generations is $E_h = (2/3)^n E_0$ (in each interaction $\sim 2/3$ of the energy is transferred to the hadronic component[25]), meaning the electromagnetic shower has $E_{EM} = E_0 -$

E_h.
After n^* generations, the energy will eventually become smaller than E_{dec}, so that the particle will be unable to interact and will decay; this value n^* is[25]

$$n^* = \frac{ln(E_0/E_{dec})}{ln(n_h)} \tag{4.19}$$

Flux of Particles in Hadronic Showers

The flux for any particle P in an air shower will be given as

$$\frac{d\phi_P}{dX} = -\frac{\phi_P}{\rho dP} - \frac{\phi_P}{\lambda_P} + Z_{NP}\frac{\phi_N}{\lambda_N} + Z_{PP}\frac{\phi_P}{\lambda_P} \tag{4.20}$$

with X being the column depth, dP being the decay length of particle P in the laboratory frame of reference, $\phi_P \equiv \frac{d\phi_P}{dE}$ being the differential flux of P, ϕ_N the differential flux of nucleons, λ_k the particle interaction length of hadron k and

$$Z_{hk} = \int_E^\infty dE_p \frac{\phi_k(E_P)}{\phi_k(E)} \frac{\lambda_k(E)}{\lambda(E_P)} \frac{dn(k\mathcal{N} \to hY; E_P, E)}{dE} \tag{4.21}$$

where $\frac{dn(k\mathcal{N}\to hY;E_P,E)}{dE}$ is the number of hadrons h produced with energy between E and E+dE in the scattering between the nucleus $\mathcal{N}$ and the hadron k [93].
In equation 4.20 the first term on the right-hand side is the decay term, which accounts for the possible decays of particle P during its propagation in the atmosphere. The second term represents the interaction length, accounting for how likely it is that particle P will interact in the atmosphere. The last two terms are respectively the production term (accounting for the production of particles P in the atmosphere) and the regeneration term (that accounts for interactions involving particles P and nucleons which result in the production of more particles P).

We are finally ready to see how DM could be produced from hadronic air showers. In particular we can now obtain the DM's flux that will arrive at neutrino detectors.

Chapter 5

New Limits from Meson Decays in Air Showers

The decay of mesons from air showers in an hadrophilic light dark matter candidate was first studied by [14], who made a model-independent analysis considering the decay $\eta \to S\pi^0$ and $S \to \bar{\chi}\chi$. They also consider the possibility of the decay $\pi^0 \to \gamma\bar{\chi}\chi$, which is however uninteresting in our model as the pion does have no decay at tree level (from the chiral lagrangian we don't have any decay channel for the pion) or at 1-loop involving a scalar mediator (while for a vector mediator the decay could proceed similarly to the decay $\pi^0 \to \gamma\gamma$).
Following this study, [15] studied new limits for sub-GeV up-philic DM by considering the decay of η and η' mesons, producing dark matter that is detected by direct detection experiments (such as Xenon1T and Darwin).
More recently, limits for this model have been studied at PandaX-4T [16].

In this chapter we are going to repeat these analyses by considering signals at neutrino detectors such as Super-Kamiokande and KamLAND and sensitivities from JUNO, Hyper-Kamiokande and DUNE. We are also going to consider the possibility of mesons decaying off-shell ($\eta \to \pi^0\bar{\chi}\chi$) so that the mass of the mediator can be taken more freely and we can evade other strong limits, for example from collider physics or supernova cooling, as done in s[23].

5.1 Dark Matter Upscattered by Cosmic Rays

Before talking about our results, we briefly explain the basics of [23].

In [23] it was considered the possibility for cosmic rays (such as Hydrogen and Helium) to upscatter hadrophilic sub-GeV dark matter in the galaxy. This dark matter would then arrive at Earth, where it can be detected with several experiments.

They consider the cross section given in equation 3.15, which will now be used initially for High Energy CRs colliding with DM, resulting in a flux given as

$$\frac{d\phi}{d\Omega} = \sum_A \int_{l.o.s.} dL \int dK_A \frac{d\phi_A}{d\Omega} \frac{d\sigma}{dK_\chi} \frac{\rho_\chi}{m_\chi} \tag{5.1}$$

where A is either protons or helium, with their fluxes given as $d\phi_A/d\Omega$ given in figure 4.2. In this case, K_A is the kinetic energy of particle A, K_χ is the kinetic energy of DM, ρ_χ is the DM's density and m_χ its mass.
We can define the J-Factor separately as

$$J(b,l) = \int_{l.o.s.} dL \rho_\chi \tag{5.2}$$

where b and l are respectively the galactic latitude and longitude, "l.o.s." means we need to integrate on the line of sight (assuming the integration is bounded by the leaky cylinder in this case) and ρ_χ is given as the NFW profile

$$\rho_\chi = \rho_\odot \frac{r_\odot (r_\odot + r_c)^2}{r(r + r_c)^2} \tag{5.3}$$

with $r_\odot = 8.5\ kpc$ being the distance of the Sun from the Galactic Center, $r_c = 20\ kpc$ and $\rho(r = r_\odot) = 0.42\ GeV/cm^3$.

They then compute the recoil event spectrum as we will show in section 5.3, leading to new constraints and sensitivities, that are shown in figure 5.1.
We directly take from [23] the limits and constraints from collider physics and direct detection. BBNs limits are shaded as they require $m_\chi \geq 100$ MeV for our model, but can be relaxed to $m_\chi \gtrsim$ MeV by considering a coupling of the mediator to neutrinos, which is why we don't include them.

5.2 Dark Matter from Meson Decays

We now devolve our attention to the relevant instruments for our study, starting in particular with the flux of DM from meson decays.

The flux of a particle S produced during an air shower is

$$\begin{aligned}\frac{d\phi_S}{dE_S d\Omega dX} = &\sum_M \int dE_M \frac{1}{\rho(X)\lambda_M(E_M)} \times \frac{d\phi_M}{dE_M d\Omega}(E_M, \cos\theta, X) \times \\ &\times \frac{dn}{dE_S}(E_M, E_S)\end{aligned} \tag{5.4}$$

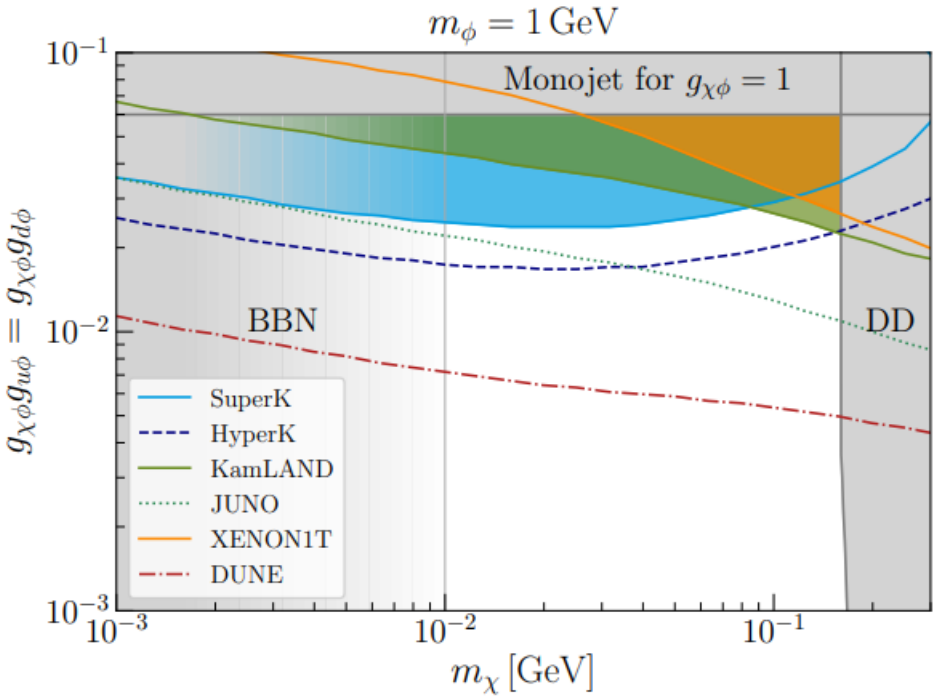

Figure 5.1 Constraints and sensitivities on $g_u g_\chi$ obtained by fixing $m_S = 1$ GeV and allowing m_χ to freely float. From [23]

where M stands for "mesons" (in this study we will consider only the η meson, but [15] considers also the η' and K^+ mesons), $E_{S,M}$ is the energy of the mediator S or the meson M, λ_M is the decay length of the meson M in the laboratory frame of reference and dn/dE_S is the particle distribution (the number n of particles S produced in the decay of M with energies between E_S and $E_S + dE_S$). For the flux of η mesons, $\frac{d\phi_M}{dE_M d\Omega}$, we consider the results from [97].
For the on-shell decay $\eta \to S + \pi^0$ equation 5.4 will be the flux of the mediators, followed by S decaying almost entirely as $S \to \bar{\chi}\chi$. This results in a Dark Matter production rate given as

$$\frac{d\phi_\chi}{dE_\chi d\Omega dX} = \int dE_S \frac{d\phi_S}{dE_S d\Omega dX} \frac{dn}{dE_S}(E_S, E_\chi) \tag{5.5}$$

This equation implies that χ and $\bar{\chi}$ are produced at the same height as the scalar mediator. If the coupling between the mediator and the dark matter isn't strong enough, the mediator may be a long-lived particle affecting the production of dark matter, which will not be the case for the coupling values of interest for this thesis.

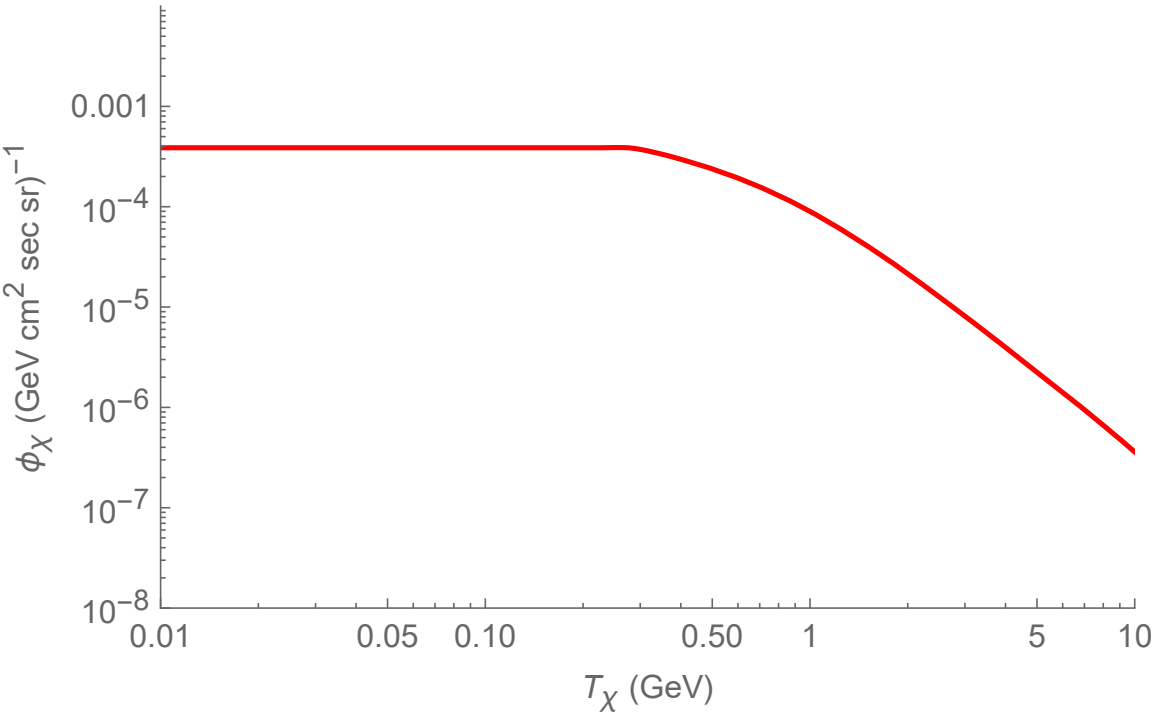

Figure 5.2 Flux of dark matter from η meson decays on-shell as a function of DM kinetic energy T_χ. In this plot the mediator mass has been taken as $m_S = 0.2\ GeV$, while $m_\chi = m_S/3$, $g_\chi = 1$ and $g_u = 10^{-3}$.

The distribution of particles for a 2-body decay $P \to P_1 P_2$ is given as

$$\frac{dn}{dE} = \frac{BR(P \to P_1 + P_2)}{p_M \sqrt{K(1; (\frac{m_1}{M})^2; (\frac{m_2}{M})^2)}} \tag{5.6}$$

where M_i with $i = 1, 2$ is the mass of particle P_i, M is the mass of particle P and K is the Kallen function. For more informations, see appendix B.1.

In the case of a three-body off-shell decay χ will be directly produced by the η (or η' or K^+, depending on how many meson species we are considering) meson decaying as $\eta \to \bar{\chi}\chi\pi^0$. In that case, in equation 5.4 the meson will decay directly to DM (instead of the mediator S), with a distribution $\frac{dn}{dE}$ that is given by following the instructions of appendix B.2.
You can see the flux of DM produced from the decays of η mesons both on-shell (figure 5.2) and off-shell (figure 5.3).

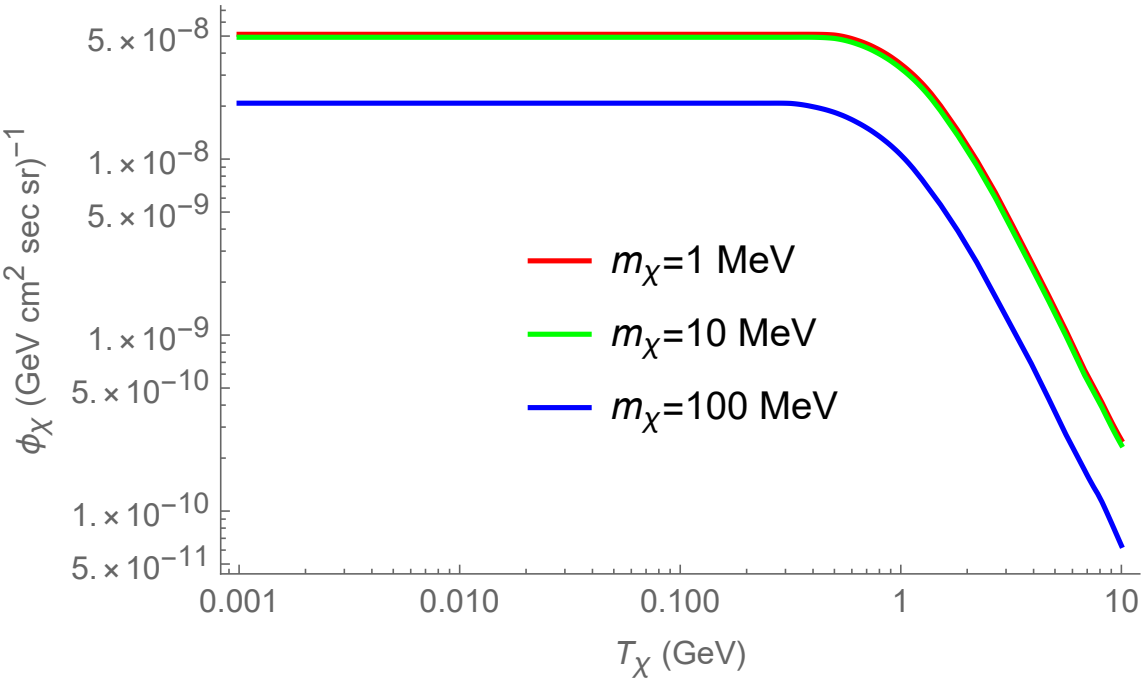

Figure 5.3 Flux of dark matter from η meson decays off-shell as a function of DM kinetic energy T_χ. In this plot the mediator mass has been taken as $ms = 1\ GeV$, while m_χ has been taken as 1, 10 and 100 MeV; in this plot $g_u g_\chi = 10^{-3}$.

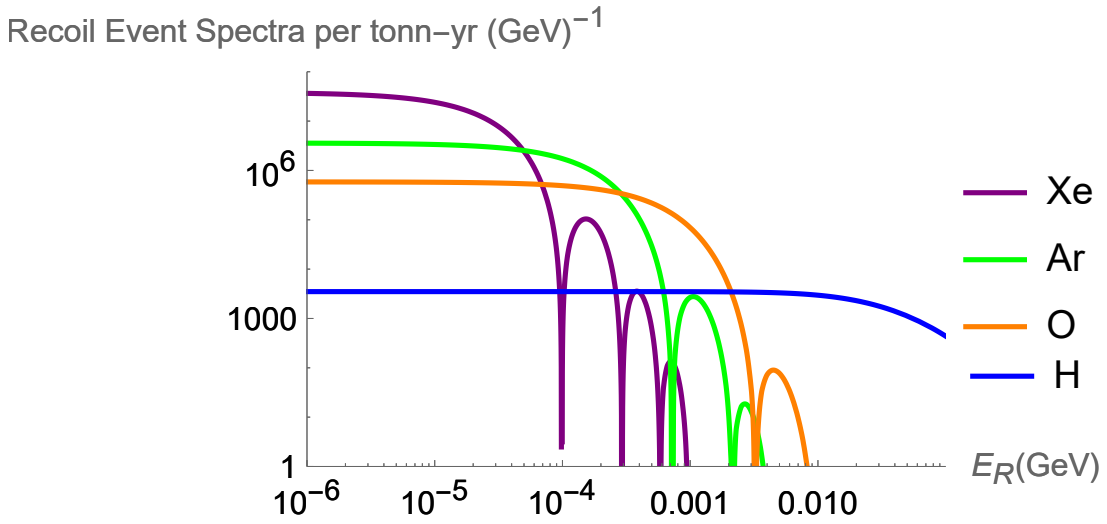

Figure 5.4 Recoil Event Spectrum for Xenon, Argon, Oxygen and Hydrogen. Here we assume $g_u = 10^{-3}$, $g_\chi = 1$, $m_S = 0.2$ GeV and $m_\chi = m_S/3$. In this figure no minimum energy for χ (that would come from the heavyside theta in the cross section) is included

5.3 Recoil Event Spectrum

The flux of DM will traverse part of the Earth and arrive at detectors, where it may interact with nuclei (or nucleons, depending on the DM energy) and produce signals. The differential event rate for a detector with N_t targets is given as

$$\frac{dN}{dT_r} = N_t \int dT_\chi \epsilon(T_r) \frac{d\sigma_{\chi N}}{dT_r} \frac{d\phi_\chi}{dT_\chi} \tag{5.7}$$

where T_r is the recoil energy of the nuclei after the interaction, T_χ is the initial kinetic energy of the dark matter, ϵ is the efficiency of the detector, $\frac{d\phi_\chi}{dT_\chi}$ is given in equation 5.5 (if the mesons decay on-shell, otherwise equation 5.4) and $\frac{d\sigma_{\chi N}}{dT_r}$ is given in equation 3.16 [23, 15, 14].
For an exposure of 1 year and 1 ton of nuclei with efficiency of 1 we obtain figure 5.4.

In figure 5.4 we can see the importance of KeV recoil energies in direct detection experiments that uses heavy nuclei (such as Xenon), while the Hydrogen spectrum tells us that higher recoil energies can be considered.

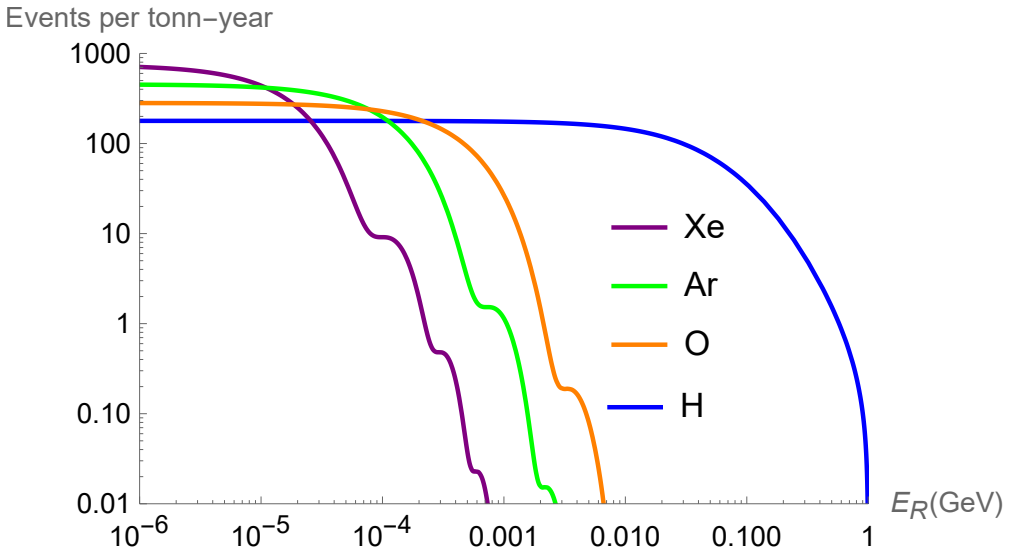

Figure 5.5 Integrated number of recoil events above a given threshold E_R. We assume $m_S = 0.2$ GeV, $g_u = 10^{-3}$, $g_\chi = 1$ and $m_S = 3m_\chi$ we still didn't include a minimum energy for χ in this plot

In figure 5.5 we finally see the integrated spectra for Xenon, Oxygen and Argon.

5.4 Attenuation

Normally any particle traversing an interacting medium will lose energy by interacting with the medium (the rock above and below the detector), resulting in an attenuation of its flux [15, 14]. This process can cause direct detection experiments to lose their sensitivity drastically (but we also highlight the possibility that some constraints may get stronger, as shown in [23], if the maximum energy threshold of the detector is smaller than the peak of the flux).

The energy loss is described by the equation

$$\frac{dT_\chi}{dz} = -\sum_N n_N \int_0^{T_R^{max}} T_r \frac{d\sigma_{\chi N}}{dT_R} dT_R \tag{5.8}$$

where n_N is the number density of target nuclei inside the Earth while the maximum energy is given as

$$T_R^{max} = \frac{T_\chi^2 + 2m_\chi T_\chi}{T_\chi + (m_\chi + m_N)^2/2m_N} \tag{5.9}$$

We can take the density of the Earth as $\rho = 2.7\ g/cm^3$ [98] and assume that all nuclei inside the Earth are Oxygen, which is the dominant component (considering $A = 12, 20, 24$ wouldn't make a change [23]).
The form factor can have relevant effects on the attenuation, in particular the form factor that we consider suppresses large momentum transfer [15].

The DM flux at a depth z is related to its value at the surface through

$$\bar{\phi}_\chi(z) d\bar{T}_\chi(z) = \phi_\chi(z=0) dT_\chi(z=0) \tag{5.10}$$

While we have developed the machinery for attenuation, we will present the results without considering it because attenuation turns out to be negligible for the small values of g_u that we will constrain.

5.5 Detectors

Once DM has traversed the Earth it will reach detectors, where it could interact resulting in detectable signals. But what detectors are we considering?
And what properties do they have?
In this section we talk about the relevant detectors and experiments considered in this study.

5.5.1 XENON1T

Built for direct dark matter searches, Xenon1T is an underground detector, operating at INFN Laboratori Nazionali del Gran Sasso, in Italy (see [99]).
The first WIMP search conducted in 2005 with Xenon10 had a target mass of 15 kg (with a fiducial mass of 5.4 kg) and was operational until 2007. It was then followed by Xenon100 with its 62 kg of target mass (and 48 kg used as fiducial volume) and lastly Xenon1T, with a target mass of 3.2t.
It is located at a depth of 3600 m water equivalent, and it was designed to detect WIMPs with masses around 50 GeV with an exposure of 2.0 t-year.

Xenon1T uses Liquid Xenon as its target due to its property of self-shielding power against external background sources (as Z=54, Xenon has a strong stopping power against external γ rays) and the presence of an A^2 scaling for the cross-section.
To study the spin-dependency of the WIMP-Nucleon cross section, the isotopes of Xenon used are generally Xenon-129 and Xenon-131 (due to Xenon-129 being a spin 1/2 fermion and Xenon-131 having a 3/2 spin).
Finally, Xenon is a scintillator, which means it will emit light from excited dimers with a wavelength of 175 nm; it is also transparent to scintillation light, enabling good signal detection efficiency.

Dual-phase time projection chambers filled with liquid Xenon measure light and charged signals independently allowing for the reconstruction of position and energy while also identifying the particles. Tipically they are built with a polytetrafluoroethylene (PTFE) frame for high reflectivity, with top and bottom planes covered with arrays of light sensors (photomultiplier tubes).
When a particle hits the Xenon and deposits energy on the nucleus, light and electrons are produced, with the light being detected by the top and bottom of the detector while electrons are drifted upwards in an electric field in order to produce a secondary scintillation light.

Lastly, Xenon1T has been upgraded to XenonnT, which started operating in 2020 with 5.9 t of target mass for a total mass of 8.6 t and a fiducial mass of 4.0 t [100]. Another future upgrade to this experiment wil be the DARWIN experiment, with a fiducial mass of 50 t.

For the purposes of this study, we consider a fiducial mass of 1.3 t for Xenon1T, with an exposure of 278.8 days and a number of event observed as $N_{90\%CL} = 3.56$ (where "90%" stands for a 90% confidence level)[14]. The energy thresholds are taken as $T_1 = 4.9\ keV$ and $T_2 = 40.9\ keV$, while the efficiency is taken as the detection efficiency from [9].

5.5.2 KamLAND

The Kamioka Liquid Scintillator Antineutrino Detector (KamLAND), located at the Kamioka Observatory in Hida, Gifu, Japan, is an underground neutrino detector situated in an old mine-shaft in the Japanese Alps. For more informations on its purpose see [101].

It consists of 1200 m^3 liquid scintillator as active neutrino target, with a balloon of transparent Nylon/EVOH(Ethylene Vinyl Alcohol) film to hold the liquid scintillator and 1800 m^3 of buffer oil to cancel the background of γ rays.
There are also 1325 17 inch-aperture Photomultiplier Tubes (PMT) and 554 20 inch PMT to measure the scintillation light, a thick stainless steel tank, and a cosmic-ray anti-counter made of 3000 m^3 of water.
It is located at a depth of 1000 m underground, surrounded by 53 nuclear reactors which emit $\bar{\nu}_e$ with typical energies of a few MeV.
These $\bar{\nu}_e$ will interact with a proton, producing a positron which emits scintillation lights when it goes through the liquid scintillator.
The neutron produced together with the positron thermalises by colliding with protons and is eventually absorbed by a proton (producing deuteron), emitting a 2.2 MeV γ-ray.

The liquid scintillator is made by 80% of normal-dodecane and 20% of pseudo-documene+1.52 g/L of PPO, where the percentages stands for "percentages in volume"[102]; since in this work we are interested in the amount of free protons (hydrogen nuclei), we use this information to compute the number of free protons for each kton of target mass.
We will follow [103] to compute limits from KamLAND data [27]: in particular, KamLAND observed one event in the bin 13.5 MeVee − 20 MeVee (with eVee standing for "electron equivalent") within an exposure of 123 kton-days, where each ton of KamLAND contains approximately 8.8×10^{31} targets of Hydrogen.

5.5.3 JUNO

The Jiangmen Underground Neutrino Observatory (JUNO) is a medium baseline experiment designed to determine neutrino mass hierarchy and to precisely measure neutrino oscillations by detecting reactor neutrinos from the nuclear power plants of Yangjiang and Taishan, located 53 km away. It is located in Kaiping, Jiangmen in Guangdong province in Southern China at a depth of around 700 m, including 270 m of granite to reduce muon background [104, 30].

JUNO consists of a water Cherenkov detector, the central detector (submerged in a water pool to be shielded from natural radioactivity from the surrounding rock and air) and a muon tracker. The central detector contains 20 kton of liquid scintillator in a spherical acrylic vessel with an inner diameter of 35.4 m supported with 590 connecting bars.
17612 20-inch PMTs and 25600 3-inch PMTs watch the light emitted by the liquid scintillator. For the bigger PMTs the photon detection efficiency is 29.1% while it is $> 24\%$ for the smaller ones[30].
The Liquid Scintillator is made out of linear alkylbenzene, generally known as "LAB", due to its excellent transparency, high flash point, low chemical reactivity, and good light yield[104].

For JUNO we are going to consider as fiducial mass 20 kton (where each kton has $\sim 8.0 \times 10^{31}$ free protons), an exposure of 5 years and the same background event rate as KamLAND[23].

5.5.4 DUNE

The Deep Underground Neutrino Experiment (DUNE) is a neutrino experiment, currently under construction, consisting of two neutrino detectors located at the Fermi National Accelerator Laboratory in Batavia, Illinois, and at the Sanford Underground Research Laboratory in Lead, South Dakota, located at approximately 1 km underground [31]. The purpose of this experiment will be the investigation of neutrino oscillation, neutrino masses, supernova neutrinos and the possible proton decays.

The accelerator in Illinois will produce a beam of neutrinos so that it will be possible to study neutrinos in the place they are produced with one detector and approximately 1300 km away, where the second detector is located.

The far detector will consist of 4 modules, each of 10 ktons of fiducial mass, 2 of which are expected to be complete by 2024 and start operating in 2026 while the other two will be operational by 2027. We assume 5 years of data-taking with a lower threshold of $T_p > 50$ MeV while the higher energy threshold can be chosen arbitrarily as long as it's much bigger than 50 MeV.
Since at these energies the DM sees nucleons, we consider for the number of targets $N_T^{DN} = 2.4 \times 10^{34}$ and assume that DUNE will be able to put limits on number of events as low as $N_{p+n}^{DN} = 30$ with a signal efficiency of 1[23].

5.5.5 Super-Kamiokande

The Super-Kamioka Neutrino Detector Experiment, also called "Super-Kamiokande", is a neutrino observatory located under Mount Ikeno in Hida, Gifu Prefecture, Japan. It's a 50 t water cherenkov detector (contained in a stainless steel tank 42 meters high and 39.3 meters in diameter, with the tank volume divided in an inner detector and an outer detector) located at a depth of about 1000 meters, with 11,146 20-inch photomultiplier tubes (PMT) in diameter that face the inner detector and 1,885 8-inch PMTs that face the outer detector [105].
In 2020 13 tons of gadolinium sulfate octahydrate ($Gd_2(SO_4)_3 \cdot 8H_2O$) were dissolved into the water tank, improving Super-Kamiokande's neutron detection efficiency while also increasing its sensitivity to the diffuse supernova neutrino background flux[26].

In this work, following [23], we are going to consider an exposure of around 2287.3 days, with 22.5 kton of fiducial mass (for a total number of $N_T^{SK} = 7.5 \times 10^{33}$ targets), using as thresholds $E_{min} = 0.485$ GeV and $E_{max} = 3.17$ GeV. The efficiency is taken as $\epsilon_{SK} = 0.55$.
In this time frame, Super-K measured $N_d = 16$ downgoing and $N_u = 13$ upgoing events; since we expect a downgoing signal from DM we assume a limit $N_{events} = (N_d - N_u) + 2\sqrt{N_d} = 11$[23].

In 2027 Hyper-Kamiokande[29] will succeed Super-Kamiokande. It will be at a depth of around 650 m and we can use $\epsilon_{HK} = 0.55$ (just as Super-K), while $N_T^{HK} = 6.2 \times 10^{34}$ targets for a run of 5 years.
We assume for Hyper-K the same background event rate as for Super-K, which means an expected limit to the number of events given as $N_{events} = 19.6$[23].

5.6 Detection

Now we finally introduce our results for the detectors considered up until now.

We can obtain new limits and sensitivities by comparing the expected number of events at a certain detector and the number of events that the detector effectively observed, a condition that can be translated as

$$N_{days} N_t \int dT_r \int dT_\chi \epsilon(T_r) \frac{d\sigma_{\chi N}}{dT_r} \frac{d\phi_\chi}{dT_\chi} \leq N_{events} \tag{5.11}$$

with N_{days} being how long the detector has been running, N_t the number of target nuclei/nucleons and N_{events} is the number of events observed by the detector, defined for each detector in the previous section.

We first consider a parameter space with $m_S < 1$ GeV, where $m_\chi = m_S/3$ and $g_\chi = 1$ [20, 15, 16]; by requiring $g_\chi \sim 1$ we ensure the mediator will decay only as $S \to \bar{\chi}\chi$ (see figure C.1 for a comparison between branching ratios of S) and will be fast enough so that S is not a long lived particle.
Part of this parameter space is already constrained (as can be seen in figure 2 from [20]), so we aim to constrain the region shown in [15].

We also consider a three body decay $\eta \to \bar{\chi}\chi\pi$ with the production of the mediator S off-shell. This allows us to fix m_S freely, as long as $m_S > \sqrt{m_\eta^2 - m_\pi^2}$.

From figure 5.6 we can see that, while direct detection experiments such as Xenon1T dominate in the low mediator mass region, increasing the value of the mass of the scalar mediator S leads to stronger constraints for the neutrino detectors.
This can be explained by noticing that the cross-section in equation 3.15 contains

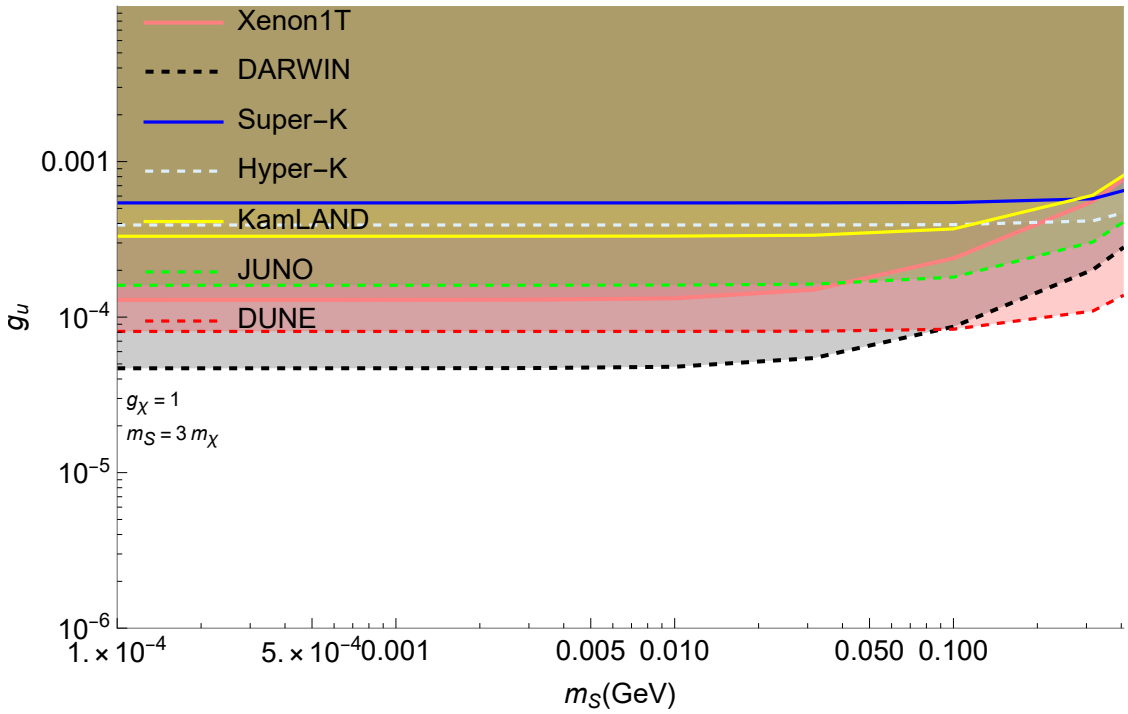

Figure 5.6 In this plot we fixed $m_S = 3m_\chi$ and $g_\chi = 1$; sensitivities are given by dashed lines, while constraints are given by thick continuous lines. Neutrino detectors generally give limits weaker than direct detection experiments for small m_S, but they get progressively stronger, leading us to believe they dominate at higher mediator masses.

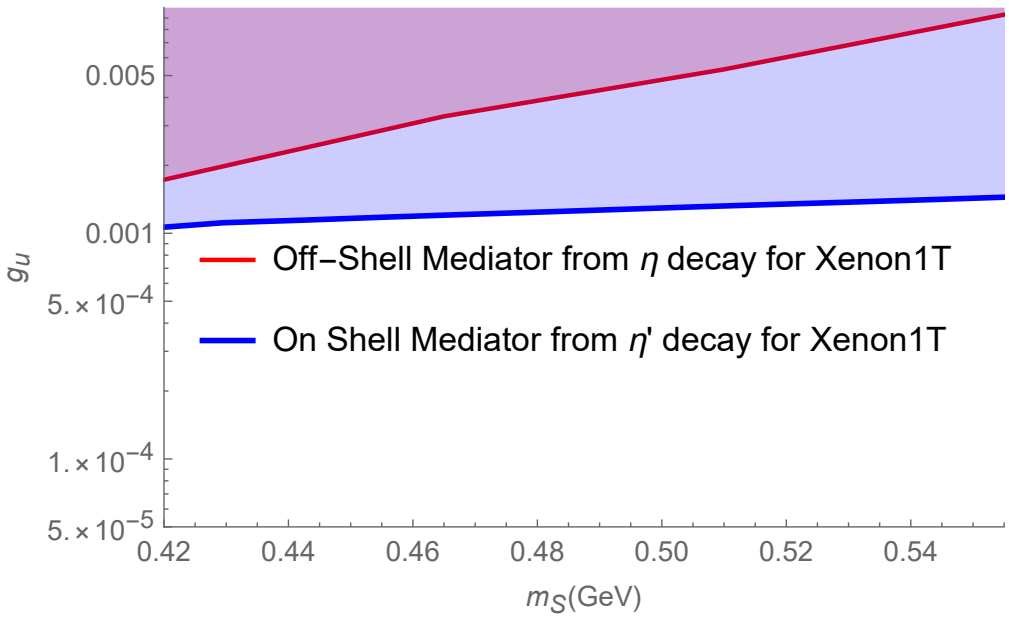

Figure 5.7 In this plot we compare Xenon1T limits from the decay of η mesons assuming the production of the mediator as a virtual particle with the analogous limits from on-shell decays of η' mesons. we see that including results from η' decay on-shell gives stronger limits in this small range of the mediator mass between $m_\eta - m_\pi$ and $m_{\eta'} - m_\pi$

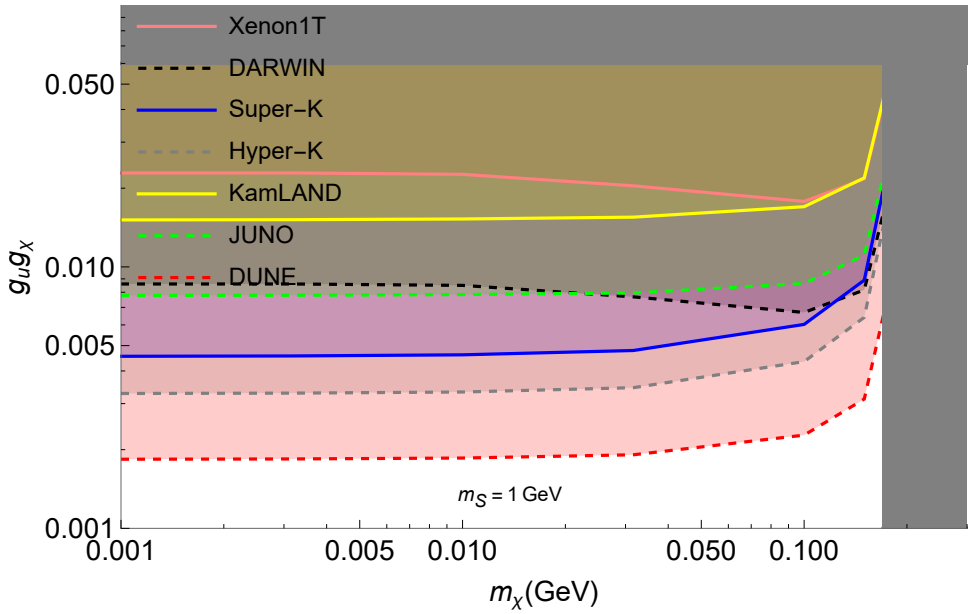

Figure 5.8 Limits and sensitivities we obtained for DM produced from atmospheric decays by fixing $m_S = 1$ GeV and allowing m_χ to float freely. Limits from monojets with $g_\chi = 1$ are displayed as the top grey band and limits from direct detection as the right gray band [23]. We didn't include limits from BBN, as they can be pushed to $m_\chi \gtrsim$ MeV by assuming a small coupling to neutrinos (see reference [23]).
If compared to figure 5.1, one can see that these limits are far stronger, with Super-Kamiokande being the world leading limit, upon which Hyper-Kamiokande and DUNE are expected to improve sensibly

a term $(2m_N T_r + m_S^2)^{-2}$; for experiments such as Xenon1T, with very low energy thresholds, m_S starts dominating earlier leading to a change of g_u as a function of m_S, which means these experiments will become less effective faster.
In particular, while Darwin is expected to give improvements over Xenon1T, DUNE would give stronger sensitivities than Darwin for $m_S \gtrsim 100$ MeV. The same happens for Xenon1T and Super-Kamiokande for $m_S \gtrsim 300$ MeV.

If we fix $m_S = 1$ GeV and allow m_χ to vary, we can consider new constraints, stronger than the ones obtained in [23]. As can be seen in figure 5.8 we obtain the strongest constraints yet for this region of the parameter space, that was mostly uncostrained prior to [23].
We see in figure 5.8 that neutrino detectors give the strongest limits possible, with Super-Kamiokande being the most efficient in constraining DM (with Hyper-Kamiokande and DUNE that should improve in a substantial way over Super-

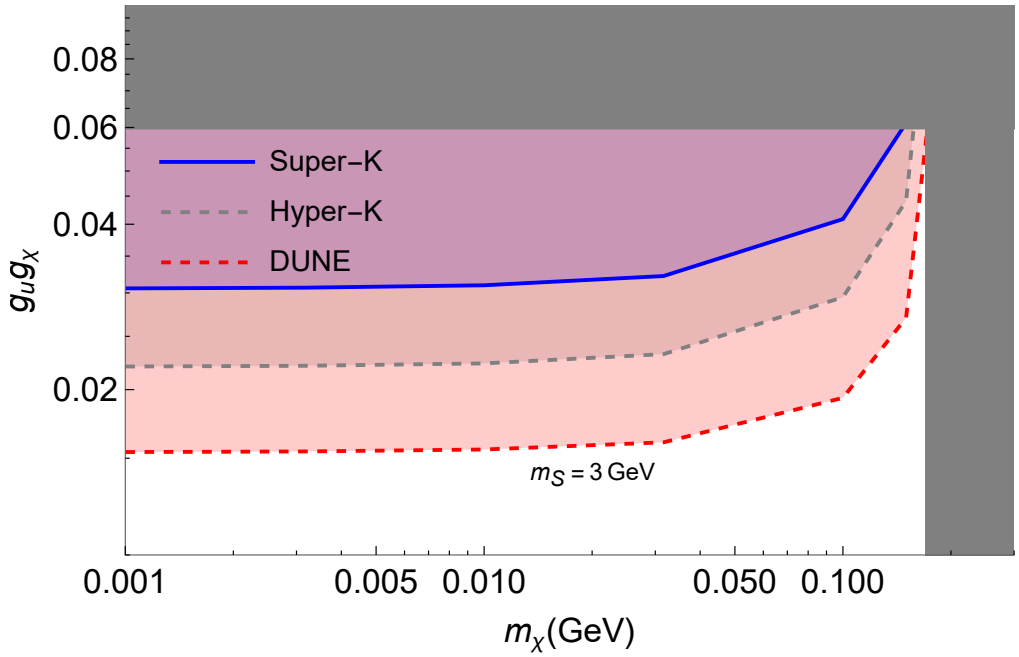

Figure 5.9 Limits and sensitivities we obtained for DM produced from atmospheric decays by fixing $m_S = 3$ GeV and allowing m_χ to float freely. Limits from monojets with $g_\chi = 1$ are displayed as the top grey band and limits from direct detection as the right gray band [23]. We didn't include limits from BBN, as they can be pushed to $m_\chi \gtrsim$ MeV by assuming a small coupling to neutrinos (see reference [23]).
If compared to the results from [23] we see that we can put limits on a region previously unconstrained

Kamiokande's limits).
It is also worth mentioning that in figure 5.9 we are able to put new limits in a region previously unconstrained from [23] by fixing $m_S = 3$ GeV and allowing m_χ to change freely.

We briefly comment figure 5.7, as it makes clear how considering the η' results may change our results in the regime where $m_S > m_\eta - m_\pi$. This would however not impact significantly the results of figure 5.8, as in [15] the flux of dark matter from η' meson decays is much smaller than the one from η meson decays.

It is imperative to notice that limits suffer from uncertainties related to the hadronic models used in the cascade equations; in particular, a possible difference of 50% could impact the flux of mesons considered, as noticed in [97].
Other possible changes could come from attenuation, as we expect our limits to be slightly weaker. However, by considering the correct form factor as [15] does,

the effect of attenuation should be small.
Since the DM signals scale as $(g_u g_\chi)^4$ (as they enter both in DM production and detection) the impact of these uncertainties on our limits in figure 5.8 and figure 5.9 is expected to be very mild.

Chapter 6

Conclusion and Discussion

The search for candidates of dark matter too light for direct detection experiments has lately attracted a lot of interest; one possible search includes the situation where this dark matter may be produced in air showers (which are the consequences of cosmic rays colliding with the atmosphere)[14], resulting in possible observable experimental signatures even at direct detection experiments such as Xenon1T[15] or PandaX[16].
Previous researches have shown however that neutrino detectors can also be effective in the detection of sub-GeV hadrophilic dark matter. In particular [23] obtains new limits from Super-Kamiokande and casts sensitivities for DUNE and Hyper-Kamiokande by looking at the component of the flux that would be upscattered by cosmic rays.
Following this approach, in this work we are able to present the strongest constraints for a sub-GeV candidate of dark matter coupled to light quarks, resulting from the decay of η mesons in the atmosphere (while [15] considered also η' and K^+). We show that neutrino detectors are more effective than typical direct detection experiments in constraining regions of the parameter space for increasing values of the mass of the scalar mediator.
In particular, by considering Super-Kamiokande data for protons detected by Cherenkov emission we are able to obtain new limits stronger than the one presented in [23] for a region of the parameter space previously unexplored by [15] and [16]. We also show that if $m_S = 3$ GeV we are able to put limits while [23] previously couldn't. It is possible to cast sensitivities for Hyper-Kamiokande and DUNE, which are expected to improve substantially over Super-K (with DUNE giving the stronger sensitivities so far).

These results motivate the realisation of the proposed searches at Super-Kamiokande, Hyper-Kamiokande and DUNE. We also remind that, for $m_S \lesssim 100$ MeV, searches at Xenon1T and Darwin could be more succesful, as direct detection experiments give stronger limits and sensitivities in that regime.

To see how we obtained these limits see chapter 5. We took the flux of η mesons in air showers from [97] and used it to obtain the flux of DM following [15], obtaining figure 5.2 and figure 5.3.
Using the cross-section obtained in section 3.2 (in particular from equation 3.16) and the flux previously seen, we could derive the event rate at detectors (see figure 5.4).
It should be noticed that for neutrino detectors the DM energies required to have a detectable signal are also enough to resolve the entire nuclear structure, so we needed to look at free protons in the detectors.
New limits and sensitivities from neutrino detectors for the region of the parameter space considered in [15] can be seen in figure 5.6, where we fixed $g_\chi = 1$ and $m_S = 3m_\chi$.
For the region of the parameter space where $m_S = 1$ GeV new limits and sensitivities can be seen in figure 5.8.
We also show limits for the region of the parameter space where $m_S = 3$ GeV in figure 5.9.

Our results are the strongest constraints yet and show the importance of large neutrino detectors in the study of light dark matter with massive mediators.
We expect to improve this results in the future by introducing the η' meson decay, which would allow us to study the region of the parameter space with $m_\eta - m_\pi < m_S < m'_\eta - m_\pi$, where decays of the η' into DM proceed via an on-shell mediator S. We then expect the resulting limits from neutrino detectors to be more constraining than those from off-shell η decays, as already seen in figure 5.7 for Xenon1T.
It will also be interesting to include new effects in the future, such as the direct production of dark matter from primary cosmic rays interacting in the atmosphere.

Appendix A

Maximum Energy

A.1 2-Body Decays Maximum Energy

In this appendix we compute the energy of a two body decay in the Center of Mass frame of reference. Let's assume we have a particle with 4-momentum $P = (M, 0, 0, 0)$ which decays into two particles with 4-momentum $P_i = (E_i, p_i, 0, 0)$ (i=1,2), so that

$$P = P_1 + P_2 \implies P - P_1 = P_2 \tag{A.1}$$

Upon squaring the previous equation, we see that, using the fact that $P_i^2 = m_i^2$:

$$M^2 + m_1^2 - 2ME_1 = m_2^2 \tag{A.2}$$

which implies that

$$E_1 = \frac{M^2 + m_1^2 - m_2^2}{2M} \tag{A.3}$$

From which we can compute the momentum p_i as

$$p_i = \sqrt{E_i^2 - m_i^2} \tag{A.4}$$

so that

$$p_1 = \frac{M}{2}\sqrt{K\left(1; \frac{m_1^2}{M^2}; \frac{m_2^2}{M^2}\right)} \tag{A.5}$$

where K is the so called "Kallen Function"[64], such that

$$K(a; b; c) = a^2 + b^2 + c^2 - 2ab - 2ac - 2bc \tag{A.6}$$

We can now change frame of reference, so that we can go into the laboratory frame, in which the decaying particle has an energy of E. Its Lorentz Factor will be $\gamma = \frac{E}{m}$ and the speed will be given by $\beta = \frac{p}{E}$ (notice that we are using c=1). Assuming a motion on a xy plane in which the speed is decomposed as $\beta_x =$

$\beta\cos(\theta)$ and $\beta_y = \beta\sin(\theta)$ we write now the Lorentz matrix

$$\Lambda = \begin{pmatrix} \gamma & \beta\gamma\cos(\theta) & \beta\gamma\sin(\theta) & 0 \\ \beta\gamma\cos(\theta) & 1+(\gamma-1)\cos(\theta)^2 & (\gamma-1)\cos(\theta)\sin(\theta) & 0 \\ \beta\gamma\sin(\theta) & (\gamma-1)\cos(\theta)\sin(\theta) & 1+(\gamma-1)\sin(\theta)^2 & 0 \\ 0 & 0 & 0 & 1 \end{pmatrix} \tag{A.7}$$

At this point we care only about the energy, so we compute it by applying ΛP, obtaining:

$$E_1' = E_1\frac{E}{M} + p_1\frac{p}{M}\cos(\theta) \tag{A.8}$$

As one can easily see, this is maximized when $\theta = 0$, so that the maximum energy will be

$$E'_{1,max} = \frac{1}{M}\left(\left(\frac{M^2+m_1^2-m_2^2}{2M}\right)E + \sqrt{E^2-M^2}\frac{M}{2}\sqrt{K\left(1;\frac{m_1^2}{M^2};\frac{m_2^2}{M^2}\right)}\right) \tag{A.9}$$

In our specific situation, we need to compute the Maximum Kinetic Energy, knowing that

$$E = T + M \tag{A.10}$$

so that

$$p = \sqrt{E^2-M^2} = \sqrt{T^2+2MT} \tag{A.11}$$

Then

$$T'_{1,max}(E,M,m_1,m_2) = \frac{1}{M}\left(\left(\frac{M^2+m_1^2-m_2^2}{2M}\right)(T+M) + \sqrt{T^2+2MT}\frac{M}{2}\sqrt{K\left(1;\frac{m_1^2}{M^2};\frac{m_2^2}{M^2}\right)}\right) - M \tag{A.12}$$

For more informations see reference [106].

A.2 3-Body Decays Maximum Energy

Following the same approach, we now compute what happens for the decay of a particle with mass M into three smaller particles with masses m_i (i=1,2,3).
Let's consider as before the conservation of 4-momenta given as:

$$P = P_1 + P_2 + P_3 \tag{A.13}$$

which means $P - P_1 = P_2 + P_3$.
We can see that the maximum value for the energy of particle 1 is achieved when particles 2 and 3 are moving in the same direction, opposite to the one of particle 1's motion. In that case we take the minimum value for their invariant mass from

[107], the value of $(P - P_1)^2 = (m_2 + m_3)^2$, so that

$$E_1{}^{MAX} = \frac{M^2 + m_1{}^2 - m_2{}^2 - m_3{}^2 - 2m_2m_3}{2M} \tag{A.14}$$

from which we can compute the momentum as

$$p_1{}^{MAX} = \sqrt{E_1{}^{MAX\,2} - m_1{}^2} = \frac{M}{2}\sqrt{K\left(1; \frac{m_1{}^2}{M^2}; \frac{m_2{}^2}{M^2}; \frac{m_3{}^2}{M^2}\right)} \tag{A.15}$$

We now go in the laboratory frame of reference, obtaining:

$$E_1'{}^{MAX} = \gamma E_1{}^{MAX} + p_1{}^{MAX}\beta\gamma \tag{A.16}$$

so that

$$E_1'{}^{MAX} = \frac{1}{M}\left(EE_1{}^{MAX} + p\sqrt{E_1{}^{MAX\,2} - m_1{}^2}\right) = \frac{EE_1{}^{MAX}}{M} + \frac{\sqrt{E^2 - M^2}}{2}\sqrt{E_1{}^{MAX\,2} - m_1{}^2} \tag{A.17}$$

where E and p are respectively the energy and the momentum of the decaying particle (as $\gamma = E/M$ and $\beta\gamma = p/M$).
For a reference where $m_1 = m_2 = 0$ see [93].

Notice that for any couple of particles, we have that $E_2 + E_3 = E - E_1{}^{MAX}$, so that $E - E_1{}^{MAX} - E_2 < E_3 < E_3{}^{MAX}$, with the smallest energy E_3 can assume always being the maximum value between $E - E_2$ and m_3.

Appendix B

Energy Distributions

If we want to compute the energy distribution for each particle, we first of all need to compute the decay amplitude, given by the formula

$$d\Gamma_{P\to P_1+P_2+P_3} = \frac{|\mathcal{M}|^2}{2m_\eta} d\Pi_{LIPS} \tag{B.1}$$

where $d\Pi_{LIPS}$ is the Lorentz Invariant Phase Space.
We can computes this phase space easily, knowing that for the three body decay of a particle P decaying into particles 1,2 and 3:

$$d\Pi_{LIPS} = \frac{1}{8(2\pi)^5}\frac{d^3p_1}{E_1}\frac{d^3p_2}{E_2}\frac{d^3p_3}{E_3}\delta^4(P - P_1 - P_2 - P_3) \tag{B.2}$$

where we use the delta to remove the integral over d^3p_3, obtaining

$$\frac{1}{8(2\pi)^5}\frac{d^3p_1}{E_1}\frac{d^3p_2}{E_2E_3}\delta(E - E_1 - E_2 - E_3) \tag{B.3}$$

We now develop $d^3p_2 = d\phi_2 d\cos\theta_{21} {p_2}^2 dp_2$, choosing for simplicity particle 1's direction of motion as the z-axis.

We can now see that ${E_3}^2 = {m_3}^2 + {p_3}^2 = {m_3}^2 + (\vec{p_1} + \vec{p_2}) \cdot (\vec{p_1} + \vec{p_2}) = {m_3}^2 + {p_1}^2 + {p_2}^2 + 2p_1p_2\cos\theta_{21}$, so that $2E_3dE_3 = 2p_1p_2 d\cos\theta_{21}$, which means that, after integrating over ϕ_2 and using the remaining delta:

$$\frac{1}{8(2\pi)^4}\frac{d^3p_1}{E_1p_1}\frac{p_2dp_2}{E_2} \tag{B.4}$$

We now develop $d^3p_1 = d\phi_1 d\cos\theta_1 {p_1}^2 dp_1$ and we integrate over the solid angle, so that we get

$$\frac{1}{4(2\pi)^3}\frac{p_1dp_1}{E_1}\frac{p_2dp_2}{E_2} = \frac{1}{4(2\pi)^3}dE_1dE_2 \tag{B.5}$$

For a reference see [107].

To compute $\Gamma_{P\to P_1+P_2+P_3}$ we would now need to integrate over the energies. To simplify the integration we can change the variables of integration to reduced energies (as done in [108]) or to dalitz variables (as done in reference [107]). For our specific study, we can keep using energies as our variables since we need to compute the energy distribution of particles which, following [93], is given as

$$\frac{dn}{dE} = \frac{BR(P \to P_1 + P_2 + P_3)}{\Gamma_{P\to P_1+P_2+P_3}} \frac{d\Gamma_{P\to P_1+P_2+P_3}}{dE} \tag{B.6}$$

where E is the energy in the laboratory frame, given as $E = \gamma\tilde{E} + \beta\gamma\tilde{p}\cos\theta$ (where in this case $\tilde{E}$ and $\tilde{p}$ are the energy and the momentum of the particle of interest in the center of mass frame).

B.1 Distribution for a 2-Body Decay

For a 2-Body decay, the differential distribution is flat on the energy in the center of mass frame, for this reason we can see that, defining $\Gamma \equiv \Gamma_{P\to P_1+P_2}$ for simplicity:

$$\frac{1}{\Gamma}\frac{d\Gamma}{dE} = \frac{1}{\Gamma}\frac{d\Gamma}{d\cos\theta}\frac{d\cos\theta}{dE} \tag{B.7}$$

where $dE = \beta\gamma\tilde{p}d\cos\theta$ (where $\tilde{p}$ is constant and we keep γ constant), so that if we consider $\beta\gamma = \frac{p_M}{M}$

$$\frac{dn}{dE} = \frac{BR(P \to P_1 + P_2)}{\Gamma}\frac{d\Gamma}{dE} = \frac{BR(P \to P_1 + P_2)}{p_M\sqrt{K\left(1; \frac{{m_1}^2}{M^2}; \frac{{m_2}^2}{M^2}\right)}} \tag{B.8}$$

as shown in [93].

B.2 Distribution for a 3-Body Decay

For a 3-Body decay what we see is that the energy in the rest frame $\tilde{E}$ is not constant. Following [109] we can however see that, defining $\Gamma \equiv \Gamma_{P\to P_1+P_2+P_3}$ for simplicity:

$$\frac{1}{\Gamma}\frac{d\Gamma}{dE} = \frac{1}{\Gamma}\int d\tilde{E}\frac{d\Gamma}{d\tilde{E}}Box(E|\gamma) \tag{B.9}$$

where the integration is weighted by the presence of a box distribution of width $E^+ - E^-$ and height $\frac{1}{E^+-E^-}$.

Appendix C

Decays of the Scalar Mediator

For $m_\chi \leq m_S/2$ the decay $S \to \chi\bar{\chi}$ is assumed (as long as g_χ isn't too small) to dominate the decays of the mediator. In this work we never consider the possibility for $m_\chi > m_S/2$, but in this case the mediator would exclusively decay to photons and hadrons, depending on its mass (if $m_S \geq 2m_\pi$ it will decay to pions, otherwise it will decay to photons). For more informations on the decays of the mediator, see reference [20].

The decay to photons happens at 1-loop (as there is no available tree-level decay), with a width given as

$$\Gamma_{S\to\gamma\gamma} = \sum_q \frac{\alpha^2 N_c^2 Q_q^4 g_q^2 m_S^3}{144\pi^3 m_q^2} \left| F_{1/2}\left(\frac{4m_q^2}{m_S^2}\right)\right|^2 \tag{C.1}$$

where N_c is the number of colors, α the fine structure constant, m_q the mass of quark q with the sum over q accounting for the possibility of the mediator to be coupled to more quarks (in this work, we however only consider the up-quark) and Q_q being the charge of said quarks. The loop function is given as

$$F_{1/2}(\tau) = \frac{3\tau}{2}\left(1 + (1-\tau)\left(\sin^{-1}\frac{1}{\sqrt{\tau}}\right)^2\right) \tag{C.2}$$

If the mediator can decay to pions the vertex $S\pi\pi$ leads to

$$\Gamma_{S\to\pi\pi} = \frac{g_u^2 B^2}{16\pi m_S}\sqrt{1 - \frac{4m_\pi^2}{m_S^2}} \tag{C.3}$$

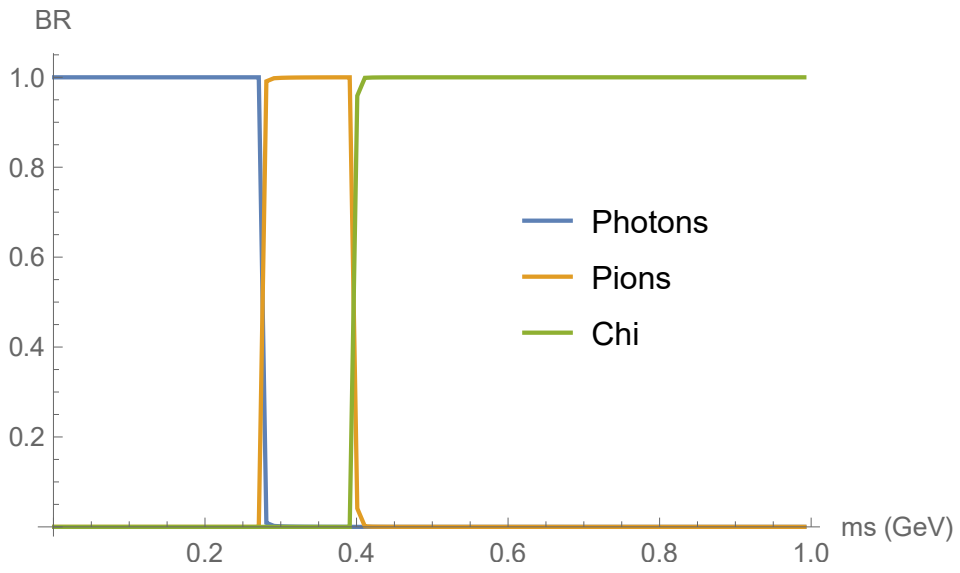

Figure C.1 Confrontation of the three discussed decays; in this case we consider $m_\chi = 200\ MeV$ to show that, as soon as it becomes available, this is the dominant decay channel assuming $g_\chi = 1$ and $g_u = 10^{-3}$

This decay is significant until kaons are kinematically accessible, as the mediator will decay through the $f_0(980)$ resonance[20]. After $m_S \gtrsim 1.3$ GeV we lose predictive power on the hadronic decays of the mediator, as more hadronic decays become accessible. Also keep in mind that other subleading terms (neglected in this width) may appear after $m_S \sim \Lambda_{QCD}$.

For the decay to dark matter, the decay width is simply given as

$$\Gamma_{S\to\chi\chi} = \frac{g_\chi^2}{8\pi} m_S \left(1 - \frac{4m_\chi^2}{m_S^2}\right)^{3/2} \tag{C.4}$$

In [20] you can find this same analysis, but with also subdominant chiral terms taken from experimental datas.

Appendix D

Birk's Law

Low energy protons will lose energy very fast due to ionization inside of liquid scintillators. There is an efficient transfer between the ionization loss of a charged particle and the detectable scintillation light, but for highly ionizing particles like low-energy protons, the light output is reduced.
This so called "quenching" follows the Birk's Law[110], which can be written as

$$E_{quenched}(T) = \int_0^T \frac{1}{1 + k_B\langle\frac{dE}{dx}\rangle + k_C\langle\frac{dE}{dx}\rangle^2} dE \tag{D.1}$$

where we call dE/dx the energy loss rate and k_B the "Birks Constant". Sometimes, to obtain a better fit, another term k_C is added in the denominator, but in this study we consider $k_C = 0$.

We take for KamLAND $k_B = 0.015$ cm/MeV [110] and for JUNO we consider $k_B = 0.0098$ cm/MeV [104], obtaining for the bin [13.5 MeVee, 20 MeVee] a recoil equivalent of [22.5 MeV,30.7 MeV] for KamLAND and [20.0 MeV,27.7 MeV] for JUNO.
Lastly, we show in figure D.1 the proton quenching at JUNO.

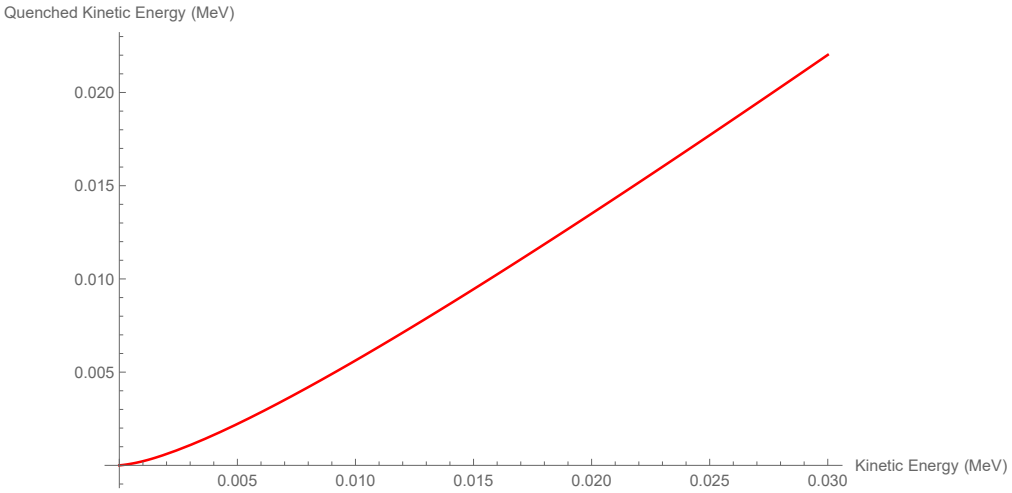

Figure D.1 Light Output from a recoiled proton at JUNO

Appendix E

Chiral Lagrangian

At large momentum transfer, QCD can be treated as a perturbative theory due to its asymptotic freedom; in the infrared however, this is not the case.
What this means is that light mesons don't look like a collection of quarks, so we need to consider the effective field theory for the interactions of the lightest hadrons. In this appendix we explain the infrared approach to QCD following [21], but for more informations you can also see [60].

Let's consider the QCD lagrangian given as

$$\mathcal{L} = \sum_{i=1}^{3} \left(\bar{q}_i i \not{D} q_i - m_i \bar{q}_i q_i \right) - \frac{1}{2} Tr G_{\mu\nu} G^{\mu\nu} \tag{E.1}$$

with the covariant derivative given as $D_\mu = \partial_\mu + igA_\mu$, $A_\mu = A^a_\mu T_a$ (T_a are the generators of SU(3)) and $G_{\mu\nu}$ being the gluon field stength.

We can clearly see that there is an invariance under $U(3)_L \times U(3)_R$, with $U(1)_A$ (where $q_i \to e^{i\alpha\gamma_5} q_i$) being a combination of these transformations that is not a symmetry of the quantum theory due to anomalies, leaving $U(1)_V \times SU(3)_L \times SU(3)_R$.
$U(1)_V$ is just the baryon number, while $SU(3)_L \times SU(3)_R$ is the so called "chiral symmetry", which is actually a broken symmetry due to the fact that the masses of quarks are not all equal.
The entity of this symmetry breaking depends on the differences between the masses, so that $SU(2)_R \times SU(2)_L$ (for up and down quarks) is not broken as badly as $SU(3)_R \times SU(3)_L$; for this reason, we can consider the isospin symmetry $SU(2)_V$ as a decent enough symmetry.

Additionally, the complexity increases if we consider the QCD vacuum spontaneously breaks the chiral $SU(3)_L \times SU(3)_R$ symmetry down to a Gell-Mann's $SU(3)_V$ through the quark condensate

$$\langle 0 | \bar{q}_{R,j} q_{L,i} | 0 \rangle = \Lambda^3 \delta_{ij} \tag{E.2}$$

where Λ has the dimension of a mass.
We can redefine the quark field through a chiral transformation $\delta_{ij} \to (LR)_{ij} \equiv \Sigma_{ij}$; if $L = R$ then $\Sigma_{ij} = \delta_{ij}$, otherwise Σ_{ij} represents a different vacuum from equation E.2 and, if $SU(3)_L \times SU(3)_R$ wasn't explicitly broken by quark masses, these two vacua would be degenerate.
By Goldstone's Theorem there would have to be 8 massless Goldstone bosons, which we can parametrized as

$$\Sigma(x) = e^{2i\pi(x)/f} \tag{E.3}$$

with $\pi = \pi^a T_a$ (T_a being the $SU(3)$ generators in the defining representation, with a=1,...,8) and f which has the dimension of a mass related to the pion decay constant.

The effective theory for the interactions of pions will have to exhibit the same chiral symmetry as QCD (invariance under $\Sigma \to L\Sigma R^\dagger$ for arbitrary matrices L,R in $SU(3)_L \times SU(3)_R$) and it must be an expansion of local operators suppressed with a cut-off Λ, set by the scale of the physics we are ignoring, so that $\Lambda \simeq 1\ GeV$.
The lowest dimension chirally symmetric operator is

$$\mathcal{L} \supset \frac{f^2}{4} Tr \partial\Sigma \partial\Sigma^\dagger \tag{E.4}$$

We find f by either considering the $\pi\pi$ scattering or through the semi-leptonic operator $\frac{1}{\sqrt{2}} G_F V_{ud} (\bar{u}\gamma^\mu(1-\gamma_5)d)(\bar{\mu}\gamma_\mu(1-\gamma_5)\nu_\mu) + h.c.$, so that the matrix element will be $\langle 0|(\bar{u}\gamma^\mu(1-\gamma_5)d)|\pi^-(p)\rangle \equiv i\sqrt{2} f_\pi p^\mu$ and we can determine f from the pion lifetime, with $f = 93\ MeV$.

To include the effects related to the quark masses, we need to include the quark mass matrix M, given as

$$M = \begin{pmatrix} m_u & 0 & 0 \\ 0 & m_d & 0 \\ 0 & 0 & m_s \end{pmatrix} \tag{E.5}$$

so that

$$\mathcal{L} \supset \Lambda^2 f^2 (\frac{c}{2\Lambda} Tr M\Sigma + h.c.) \tag{E.6}$$

where c is an unknown dimensionless coefficient with $c\Lambda \equiv B = O(\Lambda)$.
By expanding to second order in π we get that $m_\pi^2 = B(mu + md)$ so that

$$B = \frac{m_\pi^2}{m_u + m_d} \tag{E.7}$$

We now have all the tools required to finally understand how the chiral lagrangian works[21].

Appendix F

Nuclear Form Factor

In direct detection experiment, limits are generally given on the spin-independent cross section between nuclei and dark matter, which we can write as σ^{SI}. Given the mass m of dark matter and the mass M of the nucleus, we can see that the differential rate can be written as

$$\frac{dR}{dE} = \frac{\rho\sigma^{SI}}{2m\mu^2}|F(q)|^2 \int_{v>q/2\mu} \frac{f(\boldsymbol{v},t)}{v} d^3v \tag{F.1}$$

with E being the energy of the recoiling nucleus, ρ the local halo dark matter density, $q = \sqrt{2ME}$ and $f(\boldsymbol{v},t)$ the dark matter velocity distribution in the frame of the detector.
A correct determination of the form factor $F(q)$ is of vital importance to obtain the shape of the differential rate, as it contains the nuclear physics uncertainties. In this appendix we study form factors following [22, 68]. We can take the nuclear form factor to be the Fourier transform of a spherically symmetric ground state mass distribution normalized so that $F(0) = 1$ given as

$$F(q) = \frac{1}{M} \int \rho_{mass}(r) e^{-i\boldsymbol{q}\cdot\boldsymbol{r}} d^3r \tag{F.2}$$

where $\rho_{mass}(r)$ represents the mass density of the nucleus, which is difficult to probe and is generally taken so that mass and charge density are proportional, which means

$$\rho_{mass}(r) = \frac{M}{Ze}\rho_{charge}(r) \tag{F.3}$$

with $\rho_{charge}(r)$ being the charge density, determined through elastic electron scattering. Due to the normalization at $q = 0$, the proportionality establishes that $F_{mass}(q) = F_{charge}(q)$ everywhere in q.

An expression of this form factor comes from [111], where the form is given as in equation 3.17; the parameters are obtained through a fit to muon spectroscopy data[22].
New approaches to determine these parameters have been explored in the past years, fitting nuclei from ^{9}Be to ^{209}Bi, as shown in [68].

Appendix G

Branching Ratios for Meson Decays

We now show how to derive the branching ratios from section 3.2 (see references [15, 20]), starting from the effective interaction derived in section 3.1.1. Keep in mind that the decays $\eta \to S\pi^0$ and $\eta' \to S\pi^0$ are obtained in the same way.
From section 3.1.1 we see that the matrix element will be given as

$$i\mathcal{M} = ig_u BC_\eta \tag{G.1}$$

which means $|\mathcal{M}|^2 = g_u^2 B^2 C_\eta^2$.
For a 2-body decay the Lorentz Invariant Phase Space will be given as

$$d\Pi_{LIPS} = \frac{1}{(2\pi)^6}\frac{d^3p_1 d^3p_2}{2E_1 2E_2}(2\pi)^4\delta(P_1 + P_2 - P) \tag{G.2}$$

where $P_i = (E_i, \boldsymbol{p_i})$ is the 4-momentum associated to particles i=1,2 (pion and mediator), while $P = (m_\eta, \mathbf{0})$ is the 4-momentum associated to the η meson.
By using the delta function we can remove d^3p_2, while $d^3p_1 = p_1^2 d\Omega dp_1$ ($p_i = |\boldsymbol{p_i}|$).
We then have

$$d\Pi_{LIPS} = \frac{d\Omega}{16\pi^2}\frac{p_1^2 dp_1}{E_1 E_2}\delta(E_1 + E_2 - m_\eta) \tag{G.3}$$

and we know that $p_1 = p_2 \implies p_1 dp_1 = E_i dE_i$ with i=1,2.
We define $X = E_1 + E_2 - m_\eta$, so that $dX = p_1 dp_1 \frac{E_1+E_2}{E_1 E_2}$ (which means we can now change $p_1 dp_1 = dX\frac{E_1 E_2}{E_1+E_2}$)).
We now use the results from equation A.5 to finally have

$$d\Pi_{LIPS} = \frac{d\Omega p_1}{32\pi^2}\sqrt{K\left(1; \frac{m_\pi^2}{m_\eta^2}, \frac{m_S^2}{m_\eta^2}\right)} \tag{G.4}$$

If we now consider equation B.1 (that holds also for a 2-Body decay) and integrate over $d\Omega$ we see that

$$\Gamma_{\eta\to\pi^0 S} = \frac{g_u^2 B^2 C_\eta^2}{16\pi m_\eta}\sqrt{K\left(1;\frac{m_\pi^2}{m_\eta^2},\frac{m_S^2}{m_\eta^2}\right)} \tag{G.5}$$

and finally we obtain the branching ratio as $BR(\eta\to\pi^0 S) = \Gamma_{\eta\to\pi^0 S}/\Gamma_\eta$.

Bibliography

[1] V. C. Rubin, N. Thonnard, and W. K. Ford, Jr. Rotational properties of 21 SC galaxies with a large range of luminosities and radii, from NGC 4605 /R = 4kpc/ to UGC 2885 /R = 122 kpc/. *Astrophys. J.*, 238:471, 1980.

[2] N. Aghanim et al. Planck 2018 results. VI. Cosmological parameters. *Astron. Astrophys.*, 641:A6, 2020. [Erratum: Astron.Astrophys. 652, C4 (2021)].

[3] Silvia Pascoli. Neutrino physics. *CERN Yellow Rep. School Proc.*, 6:213–259, 2019.

[4] Werner Bernreuther. CP violation and baryogenesis. *Lect. Notes Phys.*, 591:237–293, 2002.

[5] C. Antel et al. Feebly Interacting Particles: FIPs 2022 workshop report. In *Workshop on Feebly-Interacting Particles*, 5 2023.

[6] Mark W. Goodman and Edward Witten. Detectability of certain dark-matter candidates. *Phys. Rev. D*, 31:3059–3063, Jun 1985.

[7] Tongyan Lin. Dark matter models and direct detection. *PoS*, 333:009, 2019.

[8] D. S. Akerib, S. Alsum, H. M. Araújo, X. Bai, A. J. Bailey, J. Balajthy, P. Beltrame, E. P. Bernard, A. Bernstein, T. P. Biesiadzinski, E. M. Boulton, R. Bramante, P. Brás, D. Byram, S. B. Cahn, M. C. Carmona-Benitez, C. Chan, A. A. Chiller, C. Chiller, A. Currie, J. E. Cutter, T. J. R. Davison, A. Dobi, J. E. Y. Dobson, E. Druszkiewicz, B. N. Edwards, C. H. Faham, S. Fiorucci, R. J. Gaitskell, V. M. Gehman, C. Ghag, K. R. Gibson, M. G. D. Gilchriese, C. R. Hall, M. Hanhardt, S. J. Haselschwardt, S. A. Hertel, D. P. Hogan, M. Horn, D. Q. Huang, C. M. Ignarra, M. Ihm, R. G. Jacobsen, W. Ji, K. Kamdin, K. Kazkaz, D. Khaitan, R. Knoche, N. A. Larsen, C. Lee, B. G. Lenardo, K. T. Lesko, A. Lindote, M. I. Lopes, A. Manalaysay, R. L. Mannino, M. F. Marzioni, D. N. McKinsey, D.-M. Mei, J. Mock, M. Moongweluwan, J. A. Morad, A. St. J. Murphy, C. Nehrkorn,

H. N. Nelson, F. Neves, K. O'Sullivan, K. C. Oliver-Mallory, K. J. Palladino, E. K. Pease, P. Phelps, L. Reichhart, C. Rhyne, S. Shaw, T. A. Shutt, C. Silva, M. Solmaz, V. N. Solovov, P. Sorensen, S. Stephenson, T. J. Sumner, M. Szydagis, D. J. Taylor, W. C. Taylor, B. P. Tennyson, P. A. Terman, D. R. Tiedt, W. H. To, M. Tripathi, L. Tvrznikova, S. Uvarov, J. R. Verbus, R. C. Webb, J. T. White, T. J. Whitis, M. S. Witherell, F. L. H. Wolfs, J. Xu, K. Yazdani, S. K. Young, and C. Zhang. Results from a search for dark matter in the complete lux exposure. *Phys. Rev. Lett.*, 118:021303, Jan 2017.

[9] E. Aprile, J. Aalbers, F. Agostini, M. Alfonsi, L. Althueser, F. D. Amaro, M. Anthony, F. Arneodo, L. Baudis, B. Bauermeister, M. L. Benabderrahmane, T. Berger, P. A. Breur, A. Brown, A. Brown, E. Brown, S. Bruenner, G. Bruno, R. Budnik, C. Capelli, J. M. R. Cardoso, D. Cichon, D. Coderre, A. P. Colijn, J. Conrad, J. P. Cussonneau, M. P. Decowski, P. de Perio, P. Di Gangi, A. Di Giovanni, S. Diglio, A. Elykov, G. Eurin, J. Fei, A. D. Ferella, A. Fieguth, W. Fulgione, A. Gallo Rosso, M. Galloway, F. Gao, M. Garbini, C. Geis, L. Grandi, Z. Greene, H. Qiu, C. Hasterok, E. Hogenbirk, J. Howlett, R. Itay, F. Joerg, B. Kaminsky, S. Kazama, A. Kish, G. Koltman, H. Landsman, R. F. Lang, L. Levinson, Q. Lin, S. Lindemann, M. Lindner, F. Lombardi, J. A. M. Lopes, J. Mahlstedt, A. Manfredini, T. Marrodán Undagoitia, J. Masbou, D. Masson, M. Messina, K. Micheneau, K. Miller, A. Molinario, K. Morå, M. Murra, J. Naganoma, K. Ni, U. Oberlack, B. Pelssers, F. Piastra, J. Pienaar, V. Pizzella, G. Plante, R. Podviianiuk, N. Priel, D. Ramírez García, L. Rauch, S. Reichard, C. Reuter, B. Riedel, A. Rizzo, A. Rocchetti, N. Rupp, J. M. F. dos Santos, G. Sartorelli, M. Scheibelhut, S. Schindler, J. Schreiner, D. Schulte, M. Schumann, L. Scotto Lavina, M. Selvi, P. Shagin, E. Shockley, M. Silva, H. Simgen, D. Thers, F. Toschi, G. Trinchero, C. Tunnell, N. Upole, M. Vargas, O. Wack, H. Wang, Z. Wang, Y. Wei, C. Weinheimer, C. Wittweg, J. Wulf, J. Ye, Y. Zhang, and T. Zhu. Dark matter search results from a one ton-year exposure of xenon1t. *Phys. Rev. Lett.*, 121:111302, Sep 2018.

[10] Xiangyi Cui, Abdusalam Abdukerim, Wei Chen, Xun Chen, Yunhua Chen, Binbin Dong, Deqing Fang, Changbo Fu, Karl Giboni, Franco Giuliani, Linhui Gu, Yikun Gu, Xuyuan Guo, Zhifan Guo, Ke Han, Changda He, Di Huang, Shengming He, Xingtao Huang, Zhou Huang, Xiangdong Ji, Yonglin Ju, Shaoli Li, Yao Li, Heng Lin, Huaxuan Liu, Jianglai Liu, Yugang Ma, Yajun Mao, Kaixiang Ni, Jinhua Ning, Xiangxiang Ren, Fang Shi, Andi Tan, Cheng Wang, Hongwei Wang, Meng Wang, Qiuhong Wang, Siguang Wang, Xiuli Wang, Xuming Wang, Qinyu Wu, Shiyong Wu, Mengjiao Xiao,

Pengwei Xie, Binbin Yan, Yong Yang, Jianfeng Yue, Dan Zhang, Hongguang Zhang, Tao Zhang, Tianqi Zhang, Li Zhao, Jifang Zhou, Ning Zhou, and Xiaopeng Zhou. Dark matter results from 54-ton-day exposure of pandax-ii experiment. *Phys. Rev. Lett.*, 119:181302, Oct 2017.

[11] Gian Francesco Giudice. The dawn of the post-naturalness era, 2017.

[12] J. Madsen. Generalized Tremaine-Gunn limits for bosons and fermions. *Phys. Rev. D*, 44:999–1006, 1991.

[13] Gianfranco Bertone and Dan Hooper. History of dark matter. *Rev. Mod. Phys.*, 90(4):045002, 2018.

[14] James Alvey, Miguel Campos, Malcolm Fairbairn, and Tevong You. Detecting Light Dark Matter via Inelastic Cosmic Ray Collisions. *Phys. Rev. Lett.*, 123:261802, 2019.

[15] Carlos A. Argüelles, Víctor Muñoz, Ian M. Shoemaker, and Volodymyr Takhistov. Hadrophilic light dark matter from the atmosphere. *Phys. Lett. B*, 833:137363, 2022.

[16] Xuyang Ning et al. Search for light dark matter from atmosphere in PandaX-4T. 1 2023.

[17] Carl D. Anderson and Seth H. Neddermeyer. Cloud chamber observations of cosmic rays at 4300 meters elevation and near sea-level. *Phys. Rev.*, 50:263–271, Aug 1936.

[18] M. Conversi, E. Pancini, and O. Piccioni. On the Disintegration of Negative Mesons. *Phys. Rev.*, 71:209–210, 1947.

[19] S. H. Neddermeyer and C. D. Anderson. Note on the Nature of Cosmic Ray Particles. *Phys. Rev.*, 51:884–886, 1937.

[20] Brian Batell, Ayres Freitas, Ahmed Ismail, and David Mckeen. Probing Light Dark Matter with a Hadrophilic Scalar Mediator. *Phys. Rev. D*, 100(9):095020, 2019.

[21] David B. Kaplan. Five lectures on effective field theory. 10 2005.

[22] Gintaras Duda, Ann Kemper, and Paolo Gondolo. Model Independent Form Factors for Spin Independent Neutralino-Nucleon Scattering from Elastic Electron Scattering Data. *JCAP*, 04:012, 2007.

[23] Yohei Ema, Filippo Sala, and Ryosuke Sato. Neutrino experiments probe hadrophilic light dark matter. *SciPost Phys.*, 10(3):072, 2021.

[24] Alessandro De Angelis and Mario Pimenta. *Introduction to Particle and Astroparticle Physics: Multimessenger Astronomy and its Particle Physics Foundations*. Undergraduate Lecture Notes in Physics. Springer Nature, Heidelberg, 2018.

[25] Maurizio Spurio. *Probes of Multimessenger Astrophysics: Charged cosmic rays, neutrinos, γ-rays and gravitational waves*. Astronomy and Astrophysics Library. Springer, 2018.

[26] K. Abe et al. First gadolinium loading to Super-Kamiokande. *Nucl. Instrum. Meth. A*, 1027:166248, 2022.

[27] S. Abe et al. Measurement of the 8B Solar Neutrino Flux with the KamLAND Liquid Scintillator Detector. *Phys. Rev. C*, 84:035804, 2011.

[28] Moritz v. Sivers. Dark Matter Search with DARWIN. In *12th Patras Workshop on Axions, WIMPs and WISPs*, pages 121–124, 2017.

[29] Masashi Yokoyama. Hyper-Kamiokande Project. In *16th Lomonosov Conference on Elementary Particle Physics*, pages 25–29, 2015.

[30] Angel Abusleme et al. JUNO physics and detector. *Prog. Part. Nucl. Phys.*, 123:103927, 2022.

[31] Babak Abi et al. Deep Underground Neutrino Experiment (DUNE), Far Detector Technical Design Report, Volume I Introduction to DUNE. *JINST*, 15(08):T08008, 2020.

[32] Daniel Baumann. *Cosmology*. Cambridge University Press, 7 2022.

[33] F. Zwicky. Die Rotverschiebung von extragalaktischen Nebeln. *Helv. Phys. Acta*, 6:110–127, 1933.

[34] David G. Cerdeno. DARK MATTER 101 From production to detection .

[35] K. Freese. Review of observational evidence for dark matter in the universe and in upcoming searches for dark stars. *EAS Publications Series*, 36:113–126, 2009.

[36] J. I. Read. The Local Dark Matter Density. *J. Phys. G*, 41:063101, 2014.

[37] Miguel Pato, Fabio Iocco, and Gianfranco Bertone. Dynamical constraints on the dark matter distribution in the milky way. *Journal of Cosmology and Astroparticle Physics*, 2015(12):001–001, dec 2015.

[38] Mariangela Lisanti. Lectures on Dark Matter Physics. In *Theoretical Advanced Study Institute in Elementary Particle Physics: New Frontiers in Fields and Strings*, pages 399–446, 2017.

[39] Douglas Clowe, Maruš a Bradač, Anthony H. Gonzalez, Maxim Markevitch, Scott W. Randall, Christine Jones, and Dennis Zaritsky. A direct empirical proof of the existence of dark matter. *The Astrophysical Journal*, 648(2):L109–L113, aug 2006.

[40] Maxim Markevitch. Chandra observation of the most interesting cluster in the universe. *ESA Spec. Publ.*, 604:723, 2006.

[41] M. Milgrom. A Modification of the Newtonian dynamics as a possible alternative to the hidden mass hypothesis. *Astrophys. J.*, 270:365–370, 1983.

[42] Kris Pardo and David N. Spergel. What is the price of abandoning dark matter? cosmological constraints on alternative gravity theories. *Physical Review Letters*, 125(21), nov 2020.

[43] Davide Guerra, Caio F.B. Macedo, and Paolo Pani. Axion boson stars. *Journal of Cosmology and Astroparticle Physics*, 2019(09):061–061, sep 2019.

[44] Ogan Özsoy and Gianmassimo Tasinato. Inflation and primordial black holes. *Universe*, 9(5):203, apr 2023.

[45] Pablo Villanueva-Domingo, Olga Mena, and Sergio Palomares-Ruiz. A brief review on primordial black holes as dark matter. *Frontiers in Astronomy and Space Sciences*, 8, may 2021.

[46] Patrick J. Fox. TASI Lectures on WIMPs and Supersymmetry. *PoS*, TASI2018:005, 2019.

[47] Pierre Jean et al. Early SPI / INTEGRAL measurements of 511 keV line emission from the 4th quadrant of the Galaxy. *Astron. Astrophys.*, 407:L55, 2003.

[48] John F. Beacom, Nicole F. Bell, and Gianfranco Bertone. Gamma-ray constraint on Galactic positron production by MeV dark matter. *Phys. Rev. Lett.*, 94:171301, 2005.

[49] Yohei Ema, Filippo Sala, and Ryosuke Sato. Dark matter models for the 511 keV galactic line predict keV electron recoils on earth. *The European Physical Journal C*, 81(2), feb 2021.

[50] Lam Hui. Wave dark matter. *Annual Review of Astronomy and Astrophysics*, 59(1):247–289, sep 2021.

[51] Luca Di Luzio, Maurizio Giannotti, Enrico Nardi, and Luca Visinelli. The landscape of QCD axion models. *Physics Reports*, 870:1–117, jul 2020.

[52] J. Aalbers et al. First Dark Matter Search Results from the LUX-ZEPLIN (LZ) Experiment. 7 2022.

[53] Ryan J. Wilkinson, Aaron C. Vincent, Cé line Bœhm, and Christopher McCabe. Ruling out the light weakly interacting massive particle explanation of the galactic 511 keV line. *Physical Review D*, 94(10), nov 2016.

[54] Nashwan Sabti, James Alvey, Miguel Escudero, Malcolm Fairbairn, and Diego Blas. Refined bounds on MeV-scale thermal dark sectors from BBN and the CMB. *Journal of Cosmology and Astroparticle Physics*, 2020(01):004–004, jan 2020.

[55] Nashwan Sabti, James Alvey, Miguel Escudero, Malcolm Fairbairn, and Diego Blas. Refined bounds on MeV-scale thermal dark sectors from BBN and the CMB. *Journal of Cosmology and Astroparticle Physics*, 2020(01):004–004, jan 2020.

[56] Guillermo Ballesteros, Marcos A. G. Garcia, and Mathias Pierre. How warm are non-thermal relics? Lyman-α bounds on out-of-equilibrium dark matter. *JCAP*, 03:101, 2021.

[57] F. Archilli, M. O. Bettler, P. Owen, and K. A. Petridis. Flavour-changing neutral currents making and breaking the standard model. *Nature*, 546(7657):221–226, 2017.

[58] Brian Batell, Ayres Freitas, Ahmed Ismail, and David Mckeen. Flavor-specific scalar mediators. *Phys. Rev. D*, 98(5):055026, 2018.

[59] Riccardo Penco. An Introduction to Effective Field Theories. 6 2020.

[60] S. Scherer. Introduction to chiral perturbation theory, 2002.

[61] A. J. MacFarlane, Anthony Sudbery, and P. H. Weisz. On Gell-Mann's lambda-matrices, d- and f-tensors, octets, and parametrizations of SU(3). *Commun. Math. Phys.*, 11:77–90, 1968.

[62] Patricia Bickert, Pere Masjuan, and Stefan Scherer. η-η' mixing in large-n_c chiral perturbation theory: discussion, phenomenology, and prospects, 2015.

[63] Martin Wolfgang Winkler. Decay and detection of a light scalar boson mixing with the Higgs boson. *Phys. Rev. D*, 99(1):015018, 2019.

[64] Gunnar Kallen. Elementary particle physics. 1964.

[65] R. L. Workman et al. Review of Particle Physics. *PTEP*, 2022:083C01, 2022.

[66] S. Durr et al. Lattice computation of the nucleon scalar quark contents at the physical point. *Phys. Rev. Lett.*, 116(17):172001, 2016.

[67] Yohei Ema, Filippo Sala, and Ryosuke Sato. Light Dark Matter at Neutrino Experiments. *Phys. Rev. Lett.*, 122(18):181802, 2019.

[68] S. E. A. Orrigo, L. Alvarez-Ruso, and C. Peña Garay. A New Approach to Nuclear Form Factors for Direct Dark Matter Searches. *Nucl. Part. Phys. Proc.*, 273-275:414–418, 2016.

[69] I. Angeli. A consistent set of nuclear rms charge radii: properties of the radius surface R(N,Z). *Atom. Data Nucl. Data Tabl.*, 87(2):185–206, 2004.

[70] Edward W Kolb and Michael Stanley Turner. *The early universe*. Frontiers in physics. Westview Press, Boulder, CO, 1990.

[71] A. Arbey and F. Mahmoudi. Dark matter and the early universe: A review. *Progress in Particle and Nuclear Physics*, 119:103865, jul 2021.

[72] Lawrence J. Hall, Karsten Jedamzik, John March-Russell, and Stephen M. West. Freeze-in production of FIMP dark matter. *Journal of High Energy Physics*, 2010(3), mar 2010.

[73] Prudhvi N. Bhattiprolu, Gilly Elor, Robert McGehee, and Aaron Pierce. Freezing-in hadrophilic dark matter at low reheating temperatures. *JHEP*, 01:128, 2023.

[74] Joachim Kopp. Collider Limits on Dark Matter. In *46th Rencontres de Moriond on Electroweak Interactions and Unified Theories*, pages 411–416, 5 2011.

[75] Lev B. Leinson. Impact of axions on the Cassiopea A neutron star cooling. *JCAP*, 09:001, 2021.

[76] Christoph Hanhart, Daniel R. Phillips, Sanjay Reddy, and Martin J. Savage. Extra dimensions, SN1987a, and nucleon-nucleon scattering data. *Nucl. Phys. B*, 595:335–359, 2001.

[77] Georg G. Raffelt. Astrophysical methods to constrain axions and other novel particle phenomena. *Physics Reports*, 198(1):1–113, 1990.

[78] Jodi Cooley. Dark Matter direct detection of classical WIMPs. *SciPost Phys. Lect. Notes*, 55:1, 2022.

[79] E. Aprile, J. Aalbers, F. Agostini, M. Alfonsi, L. Althueser, F. D. Amaro, V. C. Antochi, E. Angelino, F. Arneodo, D. Barge, L. Baudis, B. Bauermeister, L. Bellagamba, M. L. Benabderrahmane, T. Berger, P. A. Breur, A. Brown, E. Brown, S. Bruenner, G. Bruno, R. Budnik, C. Capelli, J. M.

R. Cardoso, D. Cichon, D. Coderre, A. P. Colijn, J. Conrad, J. P. Cussonneau, M. P. Decowski, P. de Perio, A. Depoian, P. Di Gangi, A. Di Giovanni, S. Diglio, A. Elykov, G. Eurin, J. Fei, A. D. Ferella, A. Fieguth, W. Fulgione, P. Gaemers, A. Gallo Rosso, M. Galloway, F. Gao, M. Garbini, L. Grandi, Z. Greene, C. Hasterok, C. Hils, E. Hogenbirk, J. Howlett, M. Iacovacci, R. Itay, F. Joerg, S. Kazama, A. Kish, M. Kobayashi, G. Koltman, A. Kopec, H. Landsman, R. F. Lang, L. Levinson, Q. Lin, S. Lindemann, M. Lindner, F. Lombardi, J. A. M. Lopes, E. López Fune, C. Macolino, J. Mahlstedt, A. Manfredini, F. Marignetti, T. Marrodán Undagoitia, J. Masbou, S. Mastroianni, M. Messina, K. Micheneau, K. Miller, A. Molinario, K. Morå, Y. Mosbacher, M. Murra, J. Naganoma, K. Ni, U. Oberlack, K. Odgers, J. Palacio, B. Pelssers, R. Peres, J. Pienaar, V. Pizzella, G. Plante, R. Podviianiuk, J. Qin, H. Qiu, D. Ramírez García, S. Reichard, B. Riedel, A. Rocchetti, N. Rupp, J. M. F. dos Santos, G. Sartorelli, N. Šarčević, M. Scheibelhut, S. Schindler, J. Schreiner, D. Schulte, M. Schumann, L. Scotto Lavina, M. Selvi, P. Shagin, E. Shockley, M. Silva, H. Simgen, C. Therreau, D. Thers, F. Toschi, G. Trinchero, C. Tunnell, N. Upole, M. Vargas, G. Volta, O. Wack, H. Wang, Y. Wei, C. Weinheimer, D. Wenz, C. Wittweg, J. Wulf, J. Ye, Y. Zhang, T. Zhu, and J. P. Zopounidis and. Light dark matter search with ionization signals in XENON1t. *Physical Review Letters*, 123(25), dec 2019.

[80] A. H. Abdelhameed, G. Angloher, P. Bauer, A. Bento, E. Bertoldo, C. Bucci, L. Canonica, A. D'Addabbo, X. Defay, S. Di Lorenzo, A. Erb, F. v. Feilitzsch, S. Fichtinger, N. Ferreiro Iachellini, A. Fuss, P. Gorla, D. Hauff, J. Jochum, A. Kinast, H. Kluck, H. Kraus, A. Langenkämper, M. Mancuso, V. Mokina, E. Mondragon, A. Münster, M. Olmi, T. Ortmann, C. Pagliarone, L. Pattavina, F. Petricca, W. Potzel, F. Pröbst, F. Reindl, J. Rothe, K. Schäffner, J. Schieck, V. Schipperges, D. Schmiedmayer, S. Schönert, C. Schwertner, M. Stahlberg, L. Stodolsky, C. Strandhagen, R. Strauss, C. Türkoğlu, I. Usherov, M. Willers, and V. Zema and. First results from the CRESST-III low-mass dark matter program. *Physical Review D*, 100(10), nov 2019.

[81] P. Agnes, I. F. M. Albuquerque, T. Alexander, A. K. Alton, G. R. Araujo, D. M. Asner, M. Ave, H. O. Back, B. Baldin, G. Batignani, K. Biery, V. Bocci, G. Bonfini, W. Bonivento, B. Bottino, F. Budano, S. Bussino, M. Cadeddu, M. Cadoni, F. Calaprice, A. Caminata, N. Canci, A. Candela, M. Caravati, M. Cariello, M. Carlini, M. Carpinelli, S. Catalanotti, V. Cataudella, P. Cavalcante, S. Cavuoti, R. Cereseto, A. Chepurnov, C. Cicalò, L. Cifarelli, A. G. Cocco, G. Covone, D. D'Angelo, M. D'Incecco, D. D'Urso, S. Davini, A. De Candia, S. De Cecco, M. De Deo, G. De Filippis, G. De Rosa, M. De Vincenzi, P. Demontis, A. V. Derbin, A. Devoto, F. Di Eu-

sanio, G. Di Pietro, C. Dionisi, M. Downing, E. Edkins, A. Empl, A. Fan, G. Fiorillo, K. Fomenko, D. Franco, F. Gabriele, A. Gabrieli, C. Galbiati, P. Garcia Abia, Chiara Ghiano, S. Giagu, C. Giganti, G. K. Giovanetti, O. Gorchakov, A. M. Goretti, F. Granato, M. Gromov, M. Guan, Y. Guardincerri, M. Gulino, B. R. Hackett, M. H. Hassanshahi, K. Herner, B. Hosseini, D. Hughes, P. Humble, E. V. Hungerford, Al. Ianni, An. Ianni, V. Ippolito, I. James, T. N. Johnson, Y. Kahn, K. Keeter, C. L. Kendziora, I. Kochanek, G. Koh, D. Korablev, G. Korga, A. Kubankin, M. Kuss, M. La Commara, M. Lai, X. Li, M. Lisanti, M. Lissia, B. Loer, G. Longo, Y. Ma, A. A. Machado, I. N. Machulin, A. Mandarano, L. Mapelli, S. M. Mari, J. Maricic, C. J. Martoff, A. Messina, P. D. Meyers, R. Milincic, S. Mishra-Sharma, A. Monte, M. Morrocchi, B. J. Mount, V. N. Muratova, P. Musico, R. Nania, A. Navrer Agasson, A. O. Nozdrina, A. Oleinik, M. Orsini, F. Ortica, L. Pagani, M. Pallavicini, L. Pandola, E. Pantic, E. Paoloni, F. Pazzona, K. Pelczar, N. Pelliccia, V. Pesudo, A. Pocar, S. Pordes, S. S. Poudel, D. A. Pugachev, H. Qian, F. Ragusa, M. Razeti, A. Razeto, B. Reinhold, A. L. Renshaw, M. Rescigno, Q. Riffard, A. Romani, B. Rossi, N. Rossi, D. Sablone, O. Samoylov, W. Sands, S. Sanfilippo, M. Sant, R. Santorelli, C. Savarese, E. Scapparone, B. Schlitzer, E. Segreto, D. A. Semenov, A. Shchagin, A. Sheshukov, P. N. Singh, M. D. Skorokhvatov, O. Smirnov, A. Sotnikov, C. Stanford, S. Stracka, G. B. Suffritti, Y. Suvorov, R. Tartaglia, G. Testera, A. Tonazzo, P. Trinchese, E. V. Unzhakov, M. Verducci, A. Vishneva, B. Vogelaar, M. Wada, T. J. Waldrop, H. Wang, Y. Wang, A. W. Watson, S. Westerdale, M. M. Wojcik, M. Wojcik, X. Xiang, X. Xiao, C. Yang, Z. Ye, C. Zhu, A. Zichichi, and G. Zuzel and. Low-mass dark matter search with the DarkSide-50 experiment. *Physical Review Letters*, 121(8), aug 2018.

[82] G. D. Rochester and C. C. Butler. Evidence for the Existence of New Unstable Elementary Particles. *Nature*, 160:855–857, 1947.

[83] Karl-Heinz Kampert, Alan A. Watson, and Alan A. Watson. Extensive Air Showers and Ultra High-Energy Cosmic Rays: A Historical Review. *Eur. Phys. J. H*, 37:359–412, 2012.

[84] M. Kachelriess. Lecture notes on high energy cosmic rays. 1 2008.

[85] J. W. Cronin, S. P. Swordy, and T. K. Gaisser. Cosmic rays at the energy frontier. *Sci. Am.*, 276:32–37, 1997.

[86] A. C. Cummings, E. C. Stone, B. C. Heikkila, N. Lal, W. R. Webber, G. Jóhannesson, I. V. Moskalenko, E. Orlando, and T. A. Porter. Galactic Cosmic Rays in the Local Interstellar Medium: Voyager 1 Observations and Model Results. *Astrophys. J.*, 831(1):18, 2016.

[87] Nicola Tomassetti, Fernando Barão, Bruna Bertucci, Emanuele Fiandrini, and Miguel Orcinha. Numerical modeling of cosmic-ray transport in the heliosphere and interpretation of the proton-to-helium ratio in solar cycle 24. *Advances in Space Research*, 64(12):2477–2489, 2019. Advances in Cosmic-Ray Astrophysics and Related Areas.

[88] M. J. Boschini, S. Della Torre, M. Gervasi, D. Grandi, G. La Vacca, S. Pensotti, P. G. Rancoita, D. Rozza, M. Tacconi, G. Jóhannesson, M. Kachelriess, N. Masi, L. Quadrani, I. V. Moskalenko, E. Orlando, T. A. Porter, and S. S. Ostapchenko. Solution of heliospheric propagation: Unveiling the local interstellar spectra of cosmic-ray species. *Astrophysical Journal*, 840(2), 5 2017.

[89] Dejan Urošević, Bojan Arbutina, and Dušan Onić. Particle acceleration in interstellar shocks. *Astrophys. Space Sci.*, 364(10):185, 2019.

[90] Marieta Bustamante, G.D.C. Montoya, W. Paula, J.A.D. Chavez, A. Gago, H. Hakobyan, P. Jez, J.A.M. Montañez, A.O. Velasquez, F.P. Cabal, M.P. Rozas, Diego Rodriguez, G.L. Romeo, U.J. Saldaña-Salazar, M. Velasquez, and M. von Steinkirch. High-energy cosmic-ray acceleration. *2009 CERN-Latin-American School of High-Energy Physics, CLASHEP 2009 - Proceedings*, pages 533–539, 01 2010.

[91] Ralph Engel, Dieter Heck, and Tanguy Pierog. Extensive air showers and hadronic interactions at high energy. *Annual Review of Nuclear and Particle Science*, 61(1):467–489, 2011.

[92] J. Knapp, D. Heck, S. J. Sciutto, M. T. Dova, and M. Risse. Extensive air shower simulations at the highest energies. *Astropart. Phys.*, 19:77–99, 2003.

[93] Carlos Argüelles, Pilar Coloma, Pilar Hernández, and Víctor Muñoz. Searches for Atmospheric Long-Lived Particles. *JHEP*, 02:190, 2020.

[94] S. Eidelman et al. Review of particle physics. Particle Data Group. *Phys. Lett. B*, 592(1-4):1, 2004.

[95] Sylvie Braibant and Giorgio Giacomelli. *Particles and fundamental interactions: An introduction to particle physics*. Undergraduate lecture notes in physics. Springer, Dordrecht, Netherlands, 2012.

[96] J. Matthews. A heitler model of extensive air showers. *Astroparticle Physics*, 22(5):387–397, 2005.

[97] Luc Darmé. Atmospheric resonant production for light dark sectors. *Phys. Rev. D*, 106(5):055015, 2022.

[98] Timon Emken and Chris Kouvaris. How blind are underground and surface detectors to strongly interacting Dark Matter? *Phys. Rev. D*, 97(11):115047, 2018.

[99] E. Aprile, , J. Aalbers, F. Agostini, M. Alfonsi, F. D. Amaro, M. Anthony, B. Antunes, F. Arneodo, M. Balata, P. Barrow, L. Baudis, B. Bauermeister, M. L. Benabderrahmane, T. Berger, A. Breskin, P. A. Breur, A. Brown, E. Brown, S. Bruenner, G. Bruno, R. Budnik, L. Bütikofer, J. Calvén, J. M. R. Cardoso, M. Cervantes, A. Chiarini, D. Cichon, D. Coderre, A. P. Colijn, J. Conrad, R. Corrieri, J. P. Cussonneau, M. P. Decowski, P. de Perio, P. Di Gangi, A. Di Giovanni, S. Diglio, J.-M. Disdier, M. Doets, E. Duchovni, G. Eurin, J. Fei, A. D. Ferella, A. Fieguth, D. Franco, D. Front, W. Fulgione, A. Gallo Rosso, M. Galloway, F. Gao, M. Garbini, C. Geis, K.-L. Giboni, L. W. Goetzke, L. Grandi, Z. Greene, C. Grignon, C. Hasterok, E. Hogenbirk, C. Huhmann, R. Itay, A. James, B. Kaminsky, S. Kazama, G. Kessler, A. Kish, H. Landsman, R. F. Lang, D. Lellouch, L. Levinson, Q. Lin, S. Lindemann, M. Lindner, F. Lombardi, J. A. M. Lopes, R. Maier, A. Manfredini, I. Maris, T. Marrodán Undagoitia, J. Masbou, F. V. Massoli, D. Masson, D. Mayani, M. Messina, K. Micheneau, A. Molinario, K. Morå, M. Murra, J. Naganoma, K. Ni, U. Oberlack, D. Orlandi, R. Othegraven, P. Pakarha, S. Parlati, B. Pelssers, R. Persiani, F. Piastra, J. Pienaar, V. Pizzella, M.-C. Piro, G. Plante, N. Priel, D. Ramírez García, L. Rauch, S. Reichard, C. Reuter, A. Rizzo, S. Rosendahl, N. Rupp, J. M. F. dos Santos, R. Saldanha, G. Sartorelli, M. Scheibelhut, S. Schindler, J. Schreiner, M. Schumann, L. Scotto Lavina, M. Selvi, P. Shagin, E. Shockley, M. Silva, H. Simgen, M. v. Sivers, M. Stern, A. Stein, D. Tatananni, L. Tatananni, D. Thers, A. Tiseni, G. Trinchero, C. Tunnell, N. Upole, M. Vargas, O. Wack, R. Walet, H. Wang, Z. Wang, Y. Wei, C. Weinheimer, C. Wittweg, J. Wulf, J. Ye, and Y. Zhang. The XENON1t dark matter experiment. *The European Physical Journal C*, 77(12), dec 2017.

[100] E. Aprile et al. First Dark Matter Search with Nuclear Recoils from the XENONnT Experiment. 3 2023.

[101] J. Maricic and J. G. Learned. The KamLAND anti-neutrino oscillation experiment. *Contemp. Phys.*, 46:1–14, 2005.

[102] F. Suekane, T. Iwamoto, H. Ogawa, O. Tajima, and H. Watanabe. An overview of the kamland 1-kiloton liquid scintillator. In *KEK - RCNP International School and Miniworkshop for Scintillating Crystals and their Applications in Particle and Nuclear Physics*, pages 279–290, 4 2004.

[103] Christopher V. Cappiello and John F. Beacom. Strong New Limits on Light Dark Matter from Neutrino Experiments. *Phys. Rev. D*, 100(10):103011, 2019. [Erratum: Phys.Rev.D 104, 069901 (2021)].

[104] Fengpeng An et al. Neutrino Physics with JUNO. *J. Phys. G*, 43(3):030401, 2016.

[105] M. Fechner et al. Kinematic reconstruction of atmospheric neutrino events in a large water Cherenkov detector with proton identification. *Phys. Rev. D*, 79:112010, 2009.

[106] Kaustubh Agashe, Roberto Franceschini, Sungwoo Hong, and Doojin Kim. Energy spectra of massive two-body decay products and mass measurement. *JHEP*, 04:151, 2016.

[107] Curtis A. Meyer. General properties of three-body decays. 2017.

[108] Hitoshi Murayama. Notes on phase space. 2007.

[109] Ryan Plestid, Volodymyr Takhistov, Yu-Dai Tsai, Torsten Bringmann, Alexander Kusenko, and Maxim Pospelov. New Constraints on Millicharged Particles from Cosmic-ray Production. *Phys. Rev. D*, 102:115032, 2020.

[110] John F. Beacom, Will M. Farr, and Petr Vogel. Detection of Supernova Neutrinos by Neutrino Proton Elastic Scattering. *Phys. Rev. D*, 66:033001, 2002.

[111] Richard H. Helm. Inelastic and Elastic Scattering of 187-Mev Electrons from Selected Even-Even Nuclei. *Phys. Rev.*, 104:1466–1475, 1956.